Electrical Engineering Department
California Polytechnic State University

Senior Project Final Report

Current Source DC-DC Converter for Undersea Fiber Optic Sensors

June 10th 2023

Richard Kwan
Andrew Armstrong
John Rodinec

Advisor: Professor Taufik

Table of Contents

Tables

Figures

Abstract

Today, there are nearly 400 cable networks spanning roughly 750,000 miles to connect our world together [1]. With thousands of miles of cable already lying on the ocean floor, with thousands more to come, many have recognized a unique opportunity in using this cable infrastructure as an attachment point for sensors to help study and monitor the ocean. Placing sensors onto a submarine cable is not a simple task; the sensors will require power that they receive from a transmission cable, from a battery, or from the submarine cable itself. Unfortunately, the existing power feed configuration for submarine cables typically only accounts for cable repeaters and their specified current requirement [2]. Therefore, a converter will be required to properly power the sensors. Because only the current is a known value (as the voltage will be variable depending on the position along the cable), a current source DC-DC converter must be used. This project entails the design and construction of a current source DC-DC converter that is intended to meet the following specifications for the sensors: step down an input current of 0.9 amps to 0.625 amps, maintain an output voltage of 24 volts, and an output power of 15 watts.

The goal of this project was to create a current-source DC-DC converter that stepped down a 0.9A input current to a 0.625A output current at 24V. The designed circuit successfully stepped down the input current to the proper output; however, further improvements will be needed to achieve the desired efficiency and output ripple specifications. Overall, the constructed circuit provides a proof of concept of the current source design that can be iterated upon for better results in the future.

Chapter 1. Introduction

The ability of humans to transfer information from one person to another is a prominent facet of human history. Even before the rise of modern civilizations, paintings, and oral traditions allowed us to share something with the next generations. Stone tablets and eventually books allowed information to be transferred in the written form. Later, the invention of the printing press allowed information to be copied and distributed at an unprecedented level. The development of the telegraph allowed information to be transmitted electrically rather than physically, speeding up the transfer of information over long distances. Advancements like radio and Wi-Fi removed the requirements for wires, instead using the air as the medium of transmission.

It is not immediately obvious, but the global connectedness that people enjoy today relies on the hundreds of thousands of miles of submarine cable that run between the continents. Figure 1-1 depicts a map of currently active and planned submarine cables across the Pacific Ocean. Each line represents the capability to transfer data from one side of the globe to the other in less than a second.

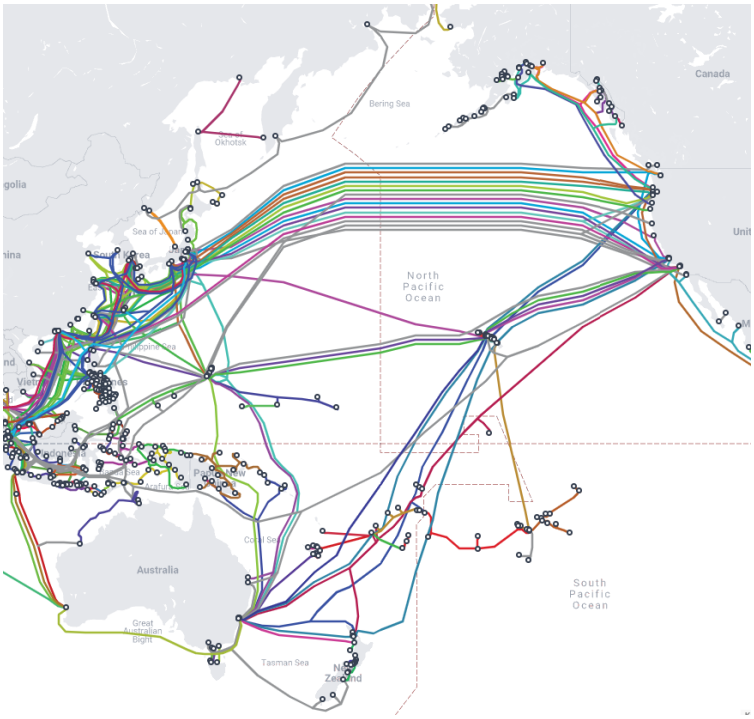

Figure 1-1. Map of submarine cables in the Pacific Ocean. [3]

The first submarine cables were telegraph cables, laid beginning in the 1850s [4]. By the 1950s, communications technology had advanced to the point that telephone submarine cables across the Atlantic were possible [4]. These telegraph and telephone cables were constructed with a metal conductor as its core to transmit information electrically. Later, an advancement was made with a new type of cable called fiber-optic cable, which uses a glass fiber, also known as optical fiber, to transmit information using light. By using light, a fiber optic cable is able to have a higher bandwidth compared to a cable using electrical signals because it can operate at a higher frequency and at longer distances without as much attenuation [5]. Figure 1-2 shows a typical construction of a submarine fiber optic cable. Note that the majority of the diameter of the cable is occupied by protective layers for insulation from the ocean as well as to give the cable structure.

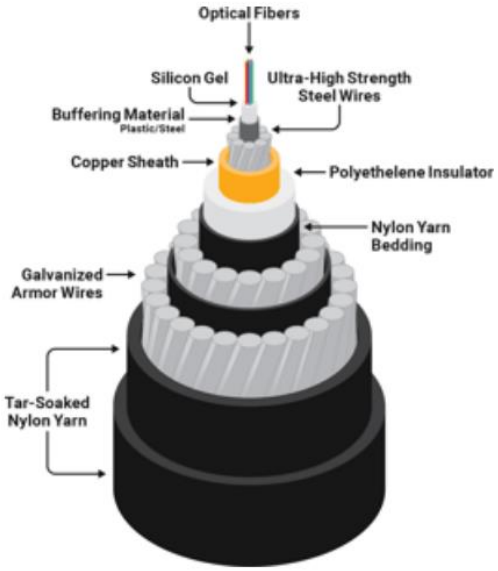

Figure 1-2. Cross section of submarine fiber optic cable. [6]

Despite the fact that fiber optic cables have less attenuation over distance than electrical cables, the large distances involved in underwater communication systems mean that even fiber optic cables require amplification after traveling a certain distance in order to preserve a signal's strength and integrity. To accomplish this, optical repeaters that amplify the signal passing through them are placed along the cable's length [7]. They are contained in pressurized vessels that go between sections of cable like the one in Figure 1-3.

Figure 1-3. Optical repeater. [8]

The repeaters, as with any other electronic device, require power in order to function. To power these repeaters, a constant current is injected at one end of the cable. This is accomplished with power feeding equipment (PFE) at the landing stations of the cable [2]. Figure 1-4 shows a block diagram of the power transmission system for optical repeaters. One landing station applies a positive voltage while the other applies a negative voltage. Because all of the repeaters are connected in series, all the repeaters see the same current. Depending on the load placed on the power feed stations, the voltages will adjust so that the current is maintained.

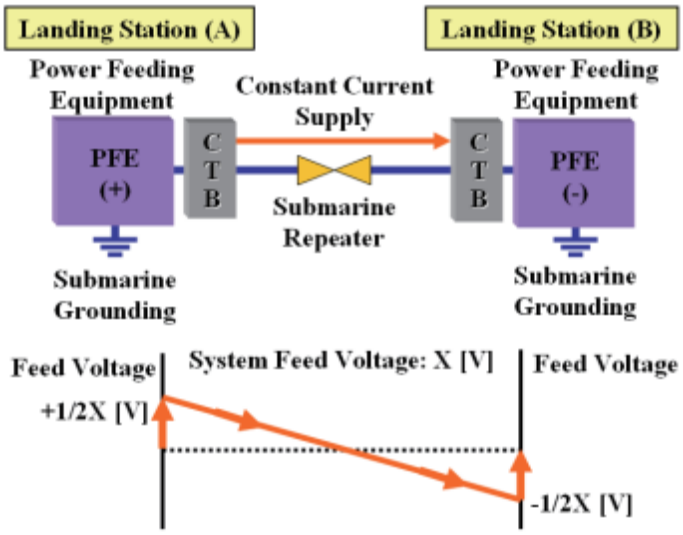

Figure 1-4. Power transmission in a submarine fiber optic cable. [2]

Note that in Figure 1-4, the voltage at any point in a fiber optic cable will not be the same as the voltage at the feed station due to the attenuation over distance.

Given the large quantities of submarine cable on the ocean floor and their ability to transmit power, many have considered the possibility of attaching sensors to these cables for the purposes of ocean monitoring. One such use case currently being explored is a tsunami early warning system. The Indonesian government is developing a Cable Based Tsunameter to replace

buoy sensors. The Cable Based Tsunameter measures acceleration, temperature, and pressure in order to detect tsunamis after a seismic or volcanic event before they reach the shore.

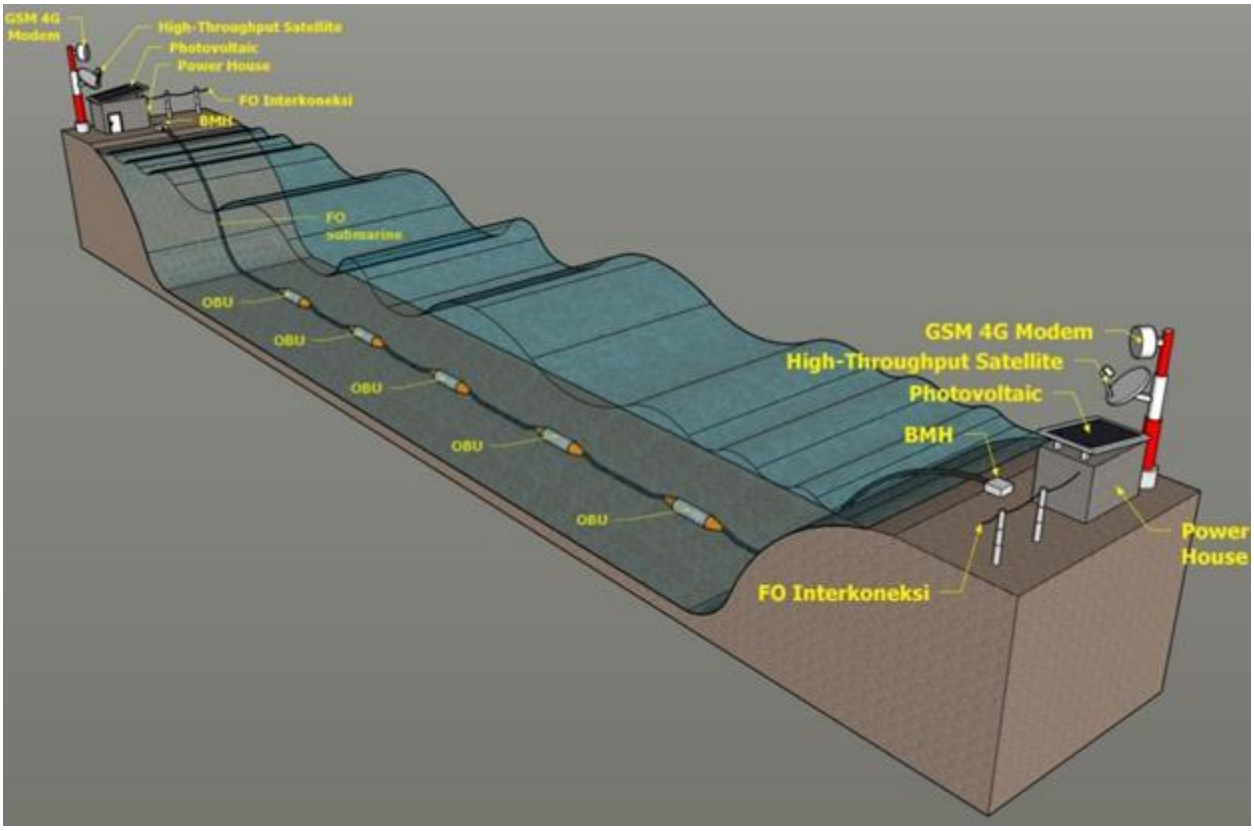

Figure 1-5. Example implementation of Cable Based Tsunameter. [9]

Figure 1-5 shows a rendering of how the Cable Based Tsunameter would be applied. The Ocean Bottom Units (OBUs) represent the pressurized vessels that will contain the sensors and/or repeaters. The land-based infrastructure on either side represents the landing stations of the cable, including the power feeding equipment.

One of the challenges with using the cable's current fed system to power the sensors is that the current is designed to match the input current specification of the repeater being used. This current value is typically around 1 A [8][10]. However, if the sensor unit requires a current that is outside of the specification of the repeater, it cannot be directly integrated into the cable without risking damage to the sensor and its associated electronics. Thus, a DC-DC converter

becomes mandatory for this kind of application to ensure that the power delivery to the sensors is at an appropriate voltage and current.

Chapter 2: Background

The majority of electronic devices today take advantage of power electronics in order to operate. Power electronics allows the conversion of power from something like a battery or a wall outlet to that required by an electronic device like a phone or microchip. Power electronic circuits are capable of performing DC-DC, DC-AC, AC-DC, and AC-AC conversion [10][11]. These circuits are what enable a single source of power to fulfill the power needs of many different types of devices. As submarine fiber optic systems are powered using DC, the focus of this project will be on DC-DC conversion.

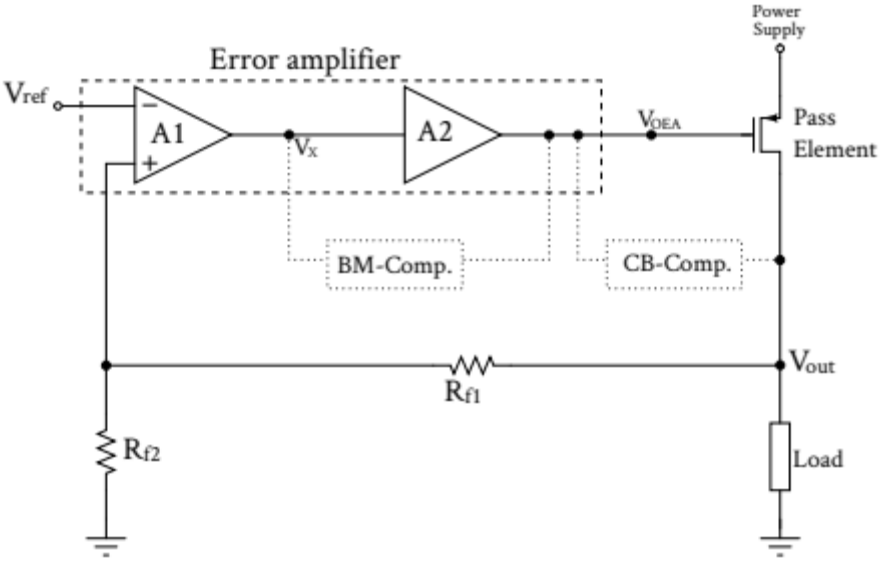

Figure 2-1: Linear Regulator Topology [12]

By far the simplest type of DC-DC conversion is a linear regulator. A linear regulator takes the input voltage and controls the pass element using the error amplifier to maintain a specific output voltage. The construction of a linear regulator is fairly simple and doesn't require complex circuitry. However, linear regulators have very poor efficiency; any input power not transferred to the load is given off as waste heat. This makes linear regulators more appropriate

for low-power devices or when there is a small difference between the input voltage and the output voltage [13]. In addition, linear regulators are only capable of stepping down the input voltage. If the voltage required by the load is higher than the input, a linear regulator cannot be used.

The alternative to linear regulators is switching regulators. Benefits of switching regulators compared to their linear counterparts are increased efficiency, smaller components, and the ability to step up voltages [14]. This is accomplished by storing and releasing energy in an inductor. On the other hand, circuit complexity and cost are increased as switching regulators require control and feedback circuitry in order to function. Switching regulators also have higher noise than linear regulators due to their constant, high-frequency switching [14].

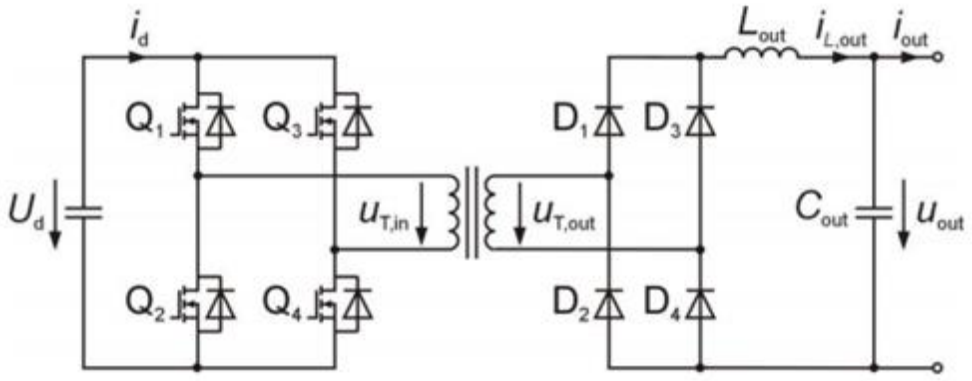

Figure 2-2: Voltage-Fed DC-DC Converter Topology [15]

Figure 2-2 illustrates the topology of a voltage-fed full-bridge DC-DC converter. Switches S_1 through S_4 are used to alternate the voltage across the primary winding of the transformer. The alternating voltage energizes the transformer and allows power to be transferred to the secondary winding. The voltage-source input imposes a limitation on this topology such that Q_1 cannot be conducted at the same time as Q_2, and Q_3 cannot be conducting at the same

time as Q_4. Doing so would shorten the input and cause a high current that would destroy the conducting circuit elements.

Due to the limitation of the way power is fed into the submarine cable, the voltage at any point along the cable with respect to ground cannot accurately be determined (see Figure 1-3). It would therefore be impractical to install a converter that is voltage-fed, given that the voltage across the terminals of any load on the cable would also be unknown unless the equivalent resistance of the converter is known. Instead, a current-fed converter should be used as the current through the cable is the only known quantity (regardless of position).

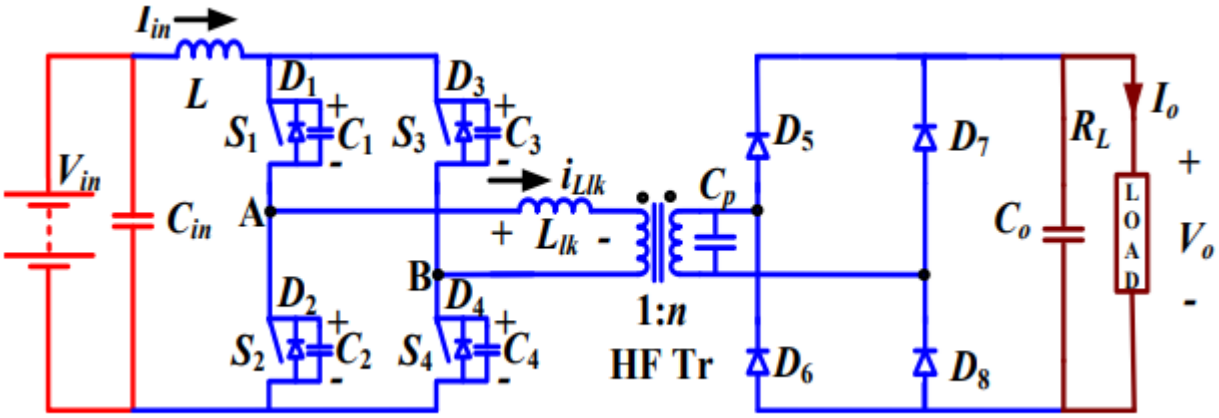

Figure 2-3: Current-Fed DC-DC Converter Topology [16]

Figure 2-3 illustrates the topology of a current-fed full-bridge DC-DC converter. Switches S_1 through S_4 are used to alternate the direction of current across the primary winding. The voltage seen across the primary winding, which is generated by the high frequency alternation of the current, is reflected across to the secondary winding, where it is then rectified with a full bridge rectifier to maintain an output voltage across the load. Furthermore, at least one of D_1 and D_3 and at least one of D_2 and D_4 must be turned on at any given moment. This is a constraint imposed by the current-source input as current may not be interrupted from the current

source. Thus, the gate drivers for D_3 and D_2 must be 180 degrees out of phase with the gate drivers for D_1 and D_4, and the duty cycle shall never drop below 50% to ensure there is a path of conduction for the input current. Failure to ensure a path of conduction will cause a large voltage spike [17].

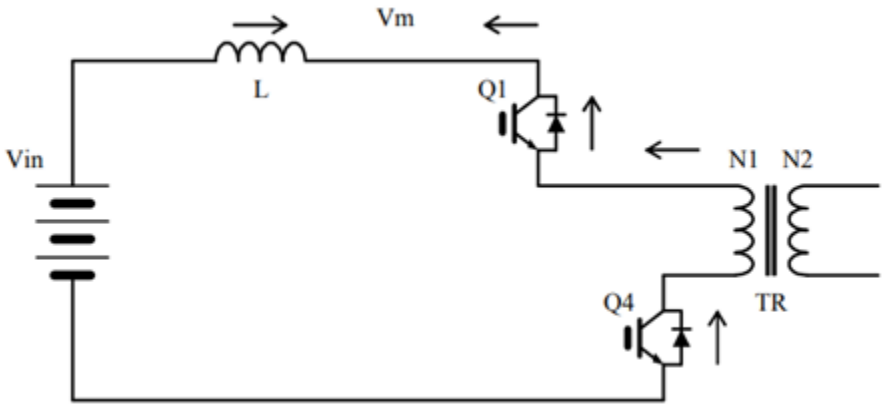

Figure 2-4: Generation of voltage spike with all switches off [17]

The current-source DC-DC converter and its potential application in submarine fiber-optic systems was previously explored in a master's thesis by Jisell Christine Jose [17]. This thesis provides the mathematical rationale behind the design choices for a current-source DC-DC converter and demonstrates the merit of such a design using circuit simulation. The circuit design provided in the thesis was able to meet the desired output electrical characteristics but noted the presence of undesired current spikes observed by some components. The thesis also suggests using a different method of modeling a transformer instead of using coupled inductors in order to get a more accurate result.

A physical version of the circuit described in the thesis was realized by Adrian Aranjo, Rocio Sanchez, and Carlos Aguilar in their report [18]. The effects of duty cycle, input current, and load resistance on the output voltage were observed; raising the duty cycle, input current,

and/or load resistance caused a rise in output voltage, and decreasing the input parameters caused a reduction in output voltage. However, the circuit failed to achieve the desired electrical output characteristics; the output voltage did not measure more than one volt, and there was negligible amount of power transferred to the load.

This project will explore the development of a current-source DC-DC converter to be used in underwater fiber-optic cable systems. This project specifically aims to build upon the aforementioned proof-of-concepts and assemble a physical circuit that can deliver the desired output electrical characteristics.

Chapter 3. Design Requirements

The high-level block diagram in Figure 3-1 shows the input and outputs of the current source DC-DC converter. The input is a 0.9A signal with unknown voltage coming from the underwater communication cables. The outputs consist of 24V DC, 0.625A DC, and 15W which are the necessary requirements to power the sensors.

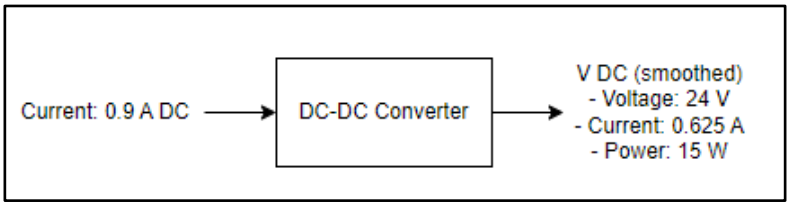

Figure 3-1. Level 0 Functional Decomposition

The current source DC-DC converter will consist of a power conversion circuit as well as a switching controller. This switching controller will take the current output voltage of the power conversion circuit and compare it against an internal reference. If there is an error between the output voltage and the reference, the controller will modify the switching signals to adjust the output voltage accordingly. Figure 3-2 illustrates how this feedback controller will interface with the DC-DC converter.

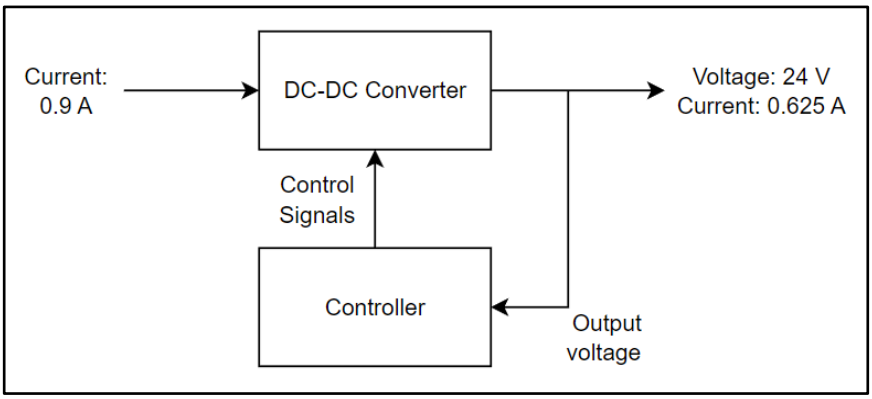

Figure 3-2. Level 1 Functional Decomposition

The DC-DC converter can be decomposed into three distinct stages. The first stage is the H-bridge. This part of the DC-DC converter will be used to convert the direct current at the input into an alternating square wave current. This alternating square wave current is applied to a transformer, which provides galvanic isolation to the output of the converter from the input and also enables the load to see a different voltage than that at the input. The galvanic isolation allows the 0.9 A current to remain uninterrupted in the feed, while providing the 0.625 A to the load. Figure 3-3 illustrates this decomposition.

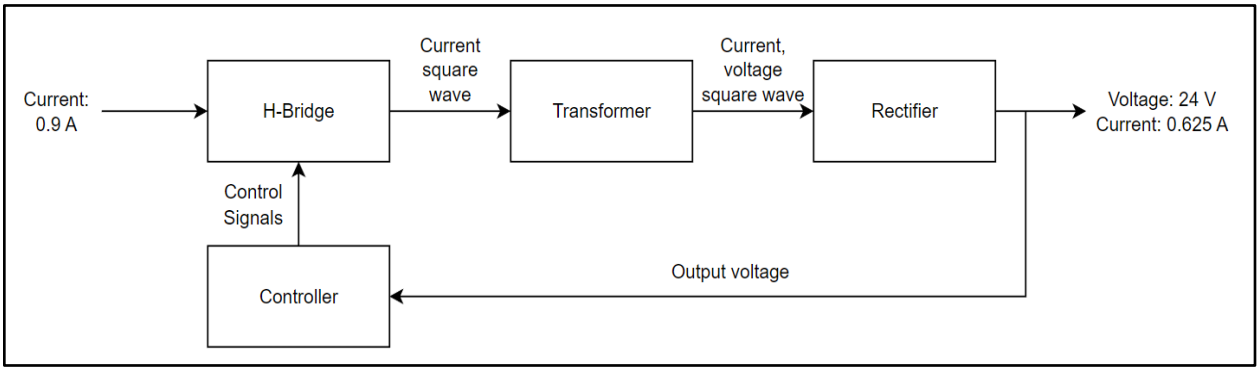

Figure 3-3. Level 2 Functional Decomposition

The converter shall have a conversion efficiency of greater than 80% at full load to minimize power draw on the input as well as dissipation of heat. Higher efficiencies will allow for the omission of heatsinks and smaller components. The output voltage ripple should be less than 3% of the output voltage. A smaller output voltage ripple means that the voltage seen by the load is more consistent, and a smaller ripple makes it less likely for overvoltage to occur. The line and load regulations of the converter shall be less than 5%. Smaller line and load regulation ensures that the output voltage remains largely consistent even when changes to the input parameters are observed. The physical dimensions of the final product shall not exceed 900 mm in length and 160 mm in width. These dimensions are approximate maximum dimensions based

on the size of a repeater unit housing provided in [10]. Table 3-1 summarizes the technical specifications for the current source converter that will be developed in this project.

Table 3-1. Engineering Specification Table

Engineering Specifications	**Value**
Electrical Specifications	
Nominal Input Current	0.9 A
Nominal Output Current	0.625 A
Average Output Voltage	24 V DC
Maximum Output Power	15 W
Output Voltage Ripple	< 3%
Power Efficiency	> 80%
Line Regulation	< 5%
Load Regulation	< 5%
Physical Specifications	
Length	900mm
Width	160mm

Chapter 4. Design and Simulation Results

The current source DC-DC converter is designed to convert an input current of 0.9A into output voltage of 24V and output current of 0.625A. This 15W output needs to remain as constant as possible in order to keep the proposed sensors properly powered. To implement these design requirements, an isolated converter system is being used with an H-bridge inverter on the primary side of the transformer and a full-bridge rectifier on the secondary side. No feedback controller is implemented in this design for simplicity, however further iterations of this project could implement one to keep the output constant and increase efficiency for various loads. A block diagram of this proposed design is shown in Figure 4-1.

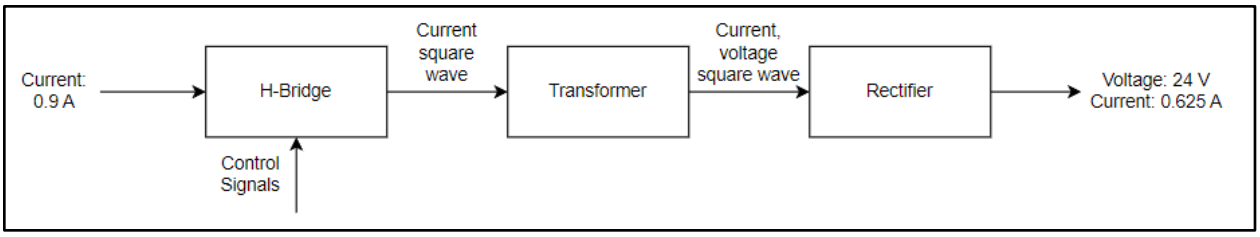

Figure 4-1: Block diagram of converter

In order to achieve the proper output characteristics, the timing of when the switches are on and off are very important. First, there should never be a time when all the switches are off, as that will cause no power to be induced at the load. The H-bridge inverter must also have a period of time when all the switches are conducting at the same time. Thus the signals that drive the switches must be out of phase of each other by 180 degrees and have a duty cycle above 50%. The following equation can be used to calculate the duty cycle of the gate driver signals.

$$\underline{\boldsymbol{V_{out}}} = \underline{\boldsymbol{V_{in}}} \frac{\boldsymbol{N_s}}{\boldsymbol{N_p}} \frac{\mathbf{1}}{\mathbf{2(1-D)}} \tag{4-1}$$

Unfortunately, V_{in} is not specified in the design requirements so this equation must be in terms of current. Thus, the following equation can be derived assuming that power into the converter

equals the power at the output. Using the design requirements of 0.9A at the input and 0.625A at the output, the ideal duty cycle for this converter would be 65.28%.

$$\frac{I_{out}}{I_{in}} = 2\frac{N_p}{N_s}(1 - D) \quad (4\text{-}2)$$

Transformer Selection

The design required the transformer to support a current of up to 0.9 A. The Wurth Elektronik 749196521 was chosen due to its flexibility, as it has three windings per side, allowing for different turns ratios. In this design, the transformer is connected such that all three windings on each side are connected in series to increase the total inductance of each transformer side. It also has current and saturation current ratings of 1.7 A and 1.73 A, which meet the necessary current requirements. In addition, this transformer had an available SPICE model from the manufacturer. Previous designs used a simple coupled inductor model in simulations, resulting in larger disparities between simulation and hardware results.

Table 4-1: 749196521 Transformer Electrical Properties

Properties		Test conditions	Value	Unit	Tol.
Inductance Base 1)	L_{BASE}	10 kHz/ 1 V	12	µH	±20%
Turns Ratio	n		1:1:1:1:1:1		
Rated Current Base 2)	$I_{R\ BASE}$	ΔT = 40 K	1.7	A	typ.
Saturation Current Base 3)	$I_{SAT\ BASE}$	IΔL/LI < 10 %	1.73	A	typ.
DC Resistance Base 4)	$R_{DC\ BASE}$	@ 20 °C	71.1	mΩ	max.
Voltage-µSecond Base 5)	$\int Udt_{\ Base}$	Unipolar waveform	98.4	µVs	max.
Leakage Inductance Base	$L_{S\ Base}$	10 kHz/ 1 V	0.24	µH	typ.
Insulation Test Voltage	V_T	3 mA/ 1 s	500	V (AC)	

Switch Selection

To determine the voltage rating of the switches, the equation 4-3 was used knowing that V_{OUT} is 24V. This means that the voltage rating of the switches has to be above 24V as a 1:1 turns ratio is being used.

$$V_{sw1} = V_{sw2} = V_{sw3} = V_{sw4} = \frac{N_p}{N_s}\underline{V_{out}} \qquad (4\text{-}3)$$

Since I_{IN} is 0.9A, the switch's current rating must be at least 0.45A using equation 4-4.

$$\underline{I_{sw1}} = \underline{I_{sw2}} = \underline{I_{sw3}} = \underline{I_{sw4}} = \underline{I_{in}}\frac{1}{2} \qquad (4\text{-}4)$$

Using this information and subsequently testing various switches on LTspice, the n-channel MOSFET BSC340N08NS3GATMA1 was chosen as it is rated for 80V and 7A. Although the ratings are higher than necessary, this switch's model was already on LTspice which made it easy to simulate and was readily available for purchase at electronics parts suppliers.

Rectifier Diode Selection

To determine the voltage rating of the rectifier diodes, equation 4-5 was used as the diodes are in parallel with the load. Thus, the voltage rating of the diodes must be at least 40V.

$$V_{D1} = V_{D2} = V_{D3} = V_{D4} = \underline{V_{out}} \qquad (4\text{-}5)$$

The current rating for the rectifier diodes were then found by using equation 4-6. Since the circuit requires a duty cycle greater than 50%, this value was used as it would yield the highest possible current that would flow through the diodes. This value ended up the same as the switches, which was 0.45A.

$$\underline{I_{D1}} = \underline{I_{D2}} = \underline{I_{D3}} = \underline{I_{D4}} = \underline{I_{in}}\frac{N_p}{N_s}(1 - D) \qquad (4\text{-}6)$$

Using this information and what was readily available to simulate on LTspice and purchase for the physical circuit, the Schottky RBR2MM40ATR diode was chosen which is rated for 40V and 2A.

Output Capacitor Selection

Using equation 4-7, a target output capacitance was determined to meet voltage ripple requirements.

$$C_1 = (\underline{I_{in}} \frac{N_p}{N_s} - \underline{I_{out}}) \frac{(1-D)}{\Delta V_o f} \quad (4\text{-}7)$$

The converter was specified to have an output voltage ripple less than 3%. With a turns ratio of 1:1, a switching frequency of 250kHz, and a duty cycle of 50%, the required output capacitance was found to be 18µF. Although the actual operating duty cycle will be higher than 50%, 50% was chosen for the calculation as it yields the highest minimum output capacitance. Three 10µF capacitors in parallel were chosen to meet this minimum output capacitance.

Snubber Components Selection

Small component values were chosen for snubber circuits, with the exception of the power rating for the snubber resistor. This is calculated as shown in Equation 4-8.

$$P_R = 0.5CV_s^2 f \quad (4\text{-}8)$$

With the switching frequency of 250 kHz and a snubber capacitance of 10 nF, the power rating of the snubber resistor was found to be at least 0.72W. However, when simulating the circuit, voltage spikes in excess of 35V were observed across the switches, which raises the requirement to 1.5W. The only available 49.9Ω resistors that met this requirement were rated at 2W, 2.5W and 6W. The 6W resistor was chosen as all three part numbers were priced similarly.

Simulation Results

Using the aforementioned components, a full schematic was created in LTspice to simulate the converter design which is shown in Figure 4-2. Although the ideal duty cycle for this converter was 65.28% based on equation 4-2, this value dropped to 58.75% due to power losses within the circuit. This duty cycle was applied to the two gate driver signals which were

operating at 250kHz and out of phase by 180 degrees. The signal timing for the LTC7062 input signals is shown in Figure 4-3.

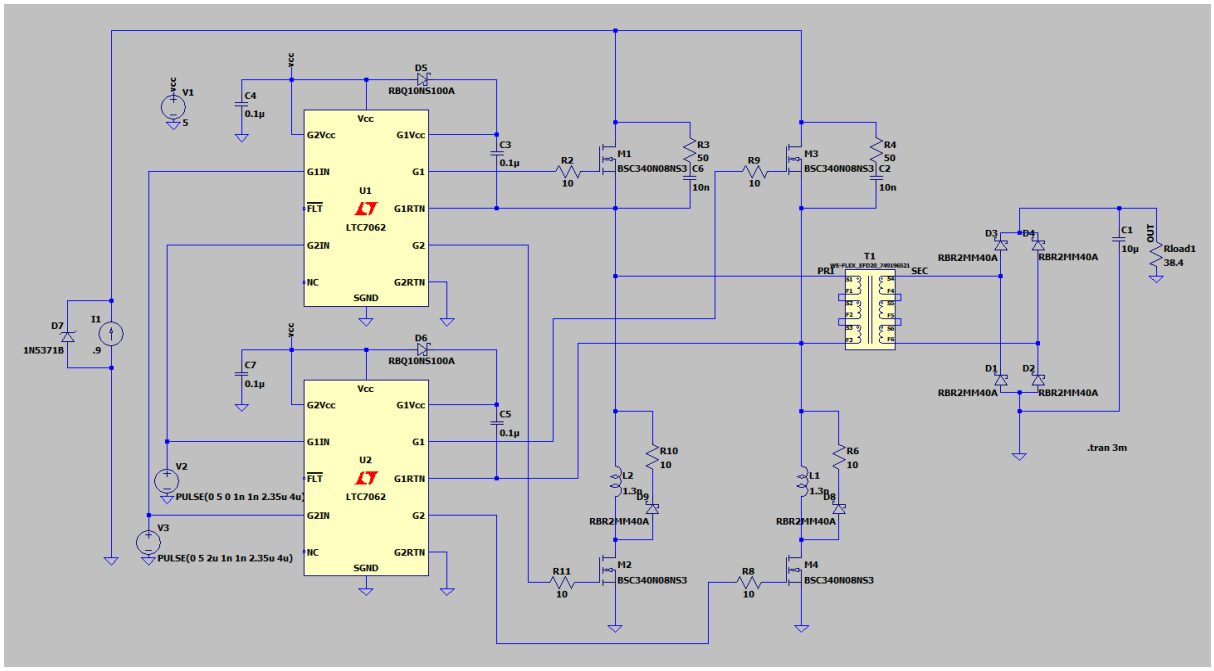

Figure 4-2 LTspice schematic of converter

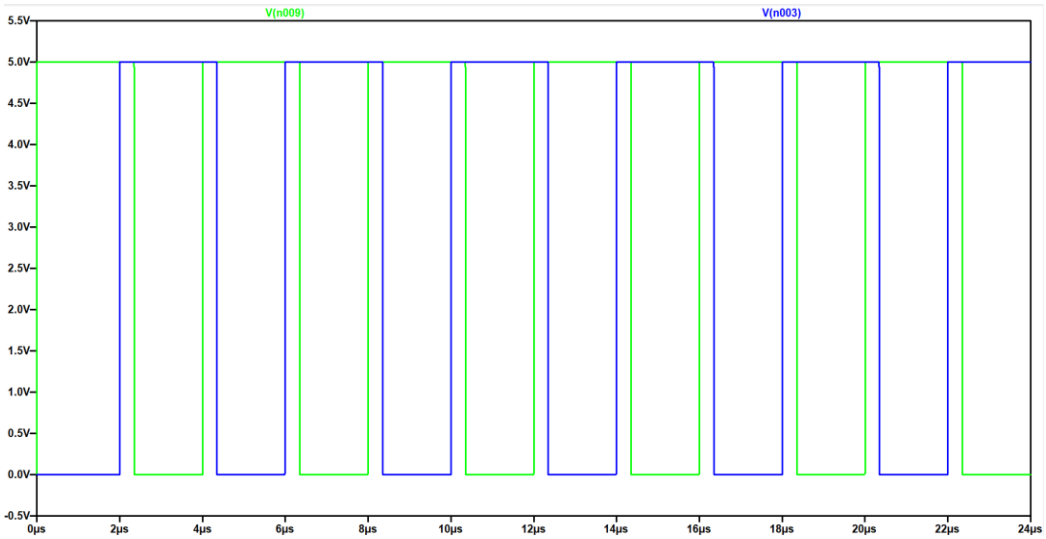

Figure 4-3 Gate Driver Input Signals

The converter was simulated for 2ms and it reached just under the desired output characteristics at 23.8V and 0.6198A as shown in Figures 4-4 and 4-5 respectively. The circuit also reached steady state in approximately 1.6ms.

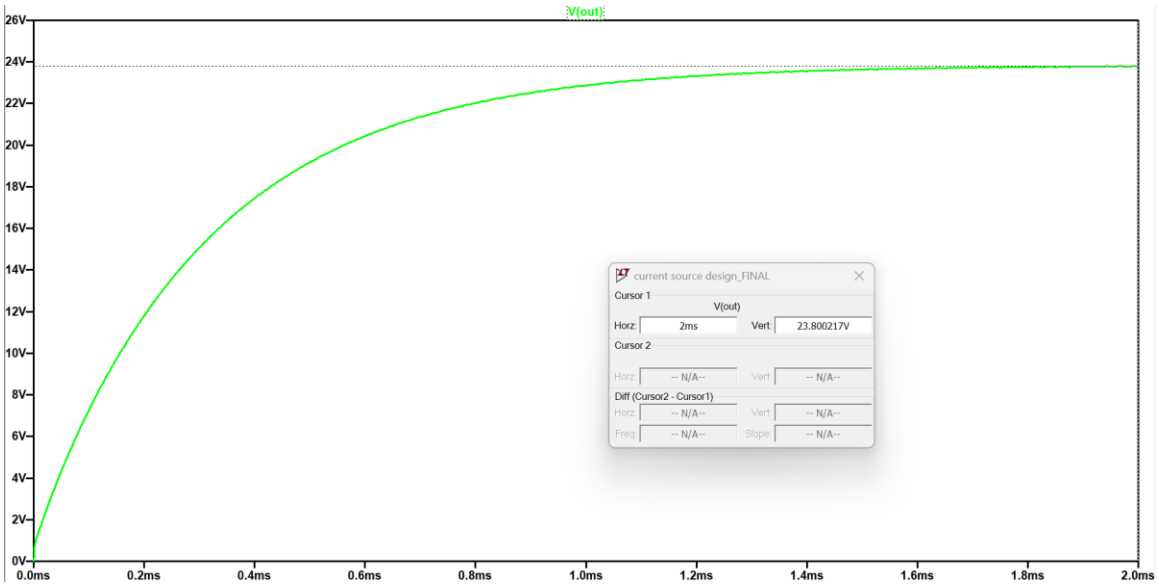

Figure 4-4: Output Voltage Waveform Simulation

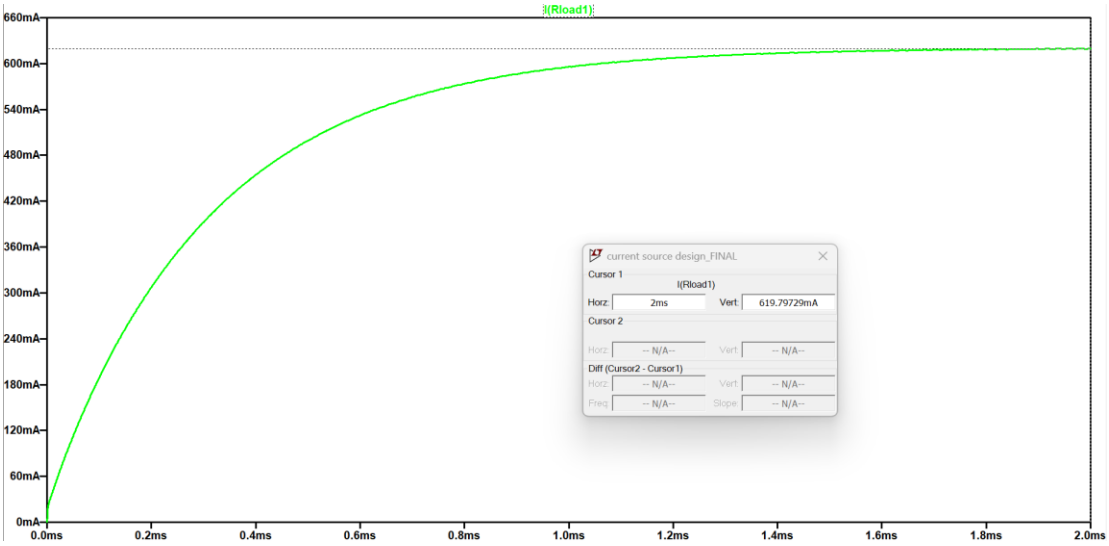

Figure 4-5: Output Current Waveform Simulation

Since the simulation provided desirable results, the Bill of Materials shown in Table 4-2 was then generated and used in the creation of the PCB layout.

Table 4-2: Bill of Materials

Part	Description	Size/Footprint	Unit Price	Quantity	Total Cost
LTC7062EMSE	Dual MOSFET Gate Driver	12-TSSOP	3.43	2	6.86
BSC340N08NS3GATMA1	N-Channel MOSFET, 80V	8-PowerTDFN	0.92	4	3.68
RB168VAM100TR	Schottky 100V 1A	2-SMD, FlatLead	0.42	2	0.84
RBR2MM40ATR	Schottky 40V 2A	SOD-123F	0.45	6	2.7
SMBJ5371B-TP	Zener 60V	DO214AA	0.48	1	0.48
749196521	Transformer, 12uH 1.7A 500VDC		10.32	1	10.32
RNCP1206FTD10R0	Resistor, 10 Ohm 1/2W +/-1%	1206	0.1	6	0.6
PCAN2512E49R9BST5	Resistor, 49.9 Ohm 6W +/0.1%	2512	7.69	2	15.38
12065C104KAT2A	Capacitor, 0.1uF 50V +/-10%	1206	0.17	4	0.68
CL21B103KCANNNC	Capacitor, 10nF 100V +/-10%	0805	0.1	2	0.2
CL31A106KBHNNNE	Capacitor, 10uF50V +/-10%	1206	0.33	3	0.99
LQW15AN1N3C80D	Inductor, 1.3nH +/-0.2nH 3.15A	0402	0.22	2	0.44
WMYCONGCONG	Banana Jack, External Thread		0.45	4	1.8
5010	Test Point, Red		0.38	12	4.56
					49.53

PCB Design

The PCB layout was created using Altium Designer. The LTSpice schematic was transferred to Altium and each component was linked to a footprint that allows for proper sizing on the board for component placement. Figure 4-6 shows the schematic for the board which was then used to generate the layout. A 2D rendering of the top and bottom layers of the board is shown in Figures 4-7 and 4-8 respectively. Some design considerations that were made included connecting the power and signal grounds only by a small thin copper trace and separating the power and signal components to opposite layers. Large copper pads were used for the power components to reduce power losses in the wiring. Figures 4-9 and 4-10 show a 3D rendering of

what the board would look like with components placed in their respective places which provided an easier way to see if the components are in an acceptable layout.

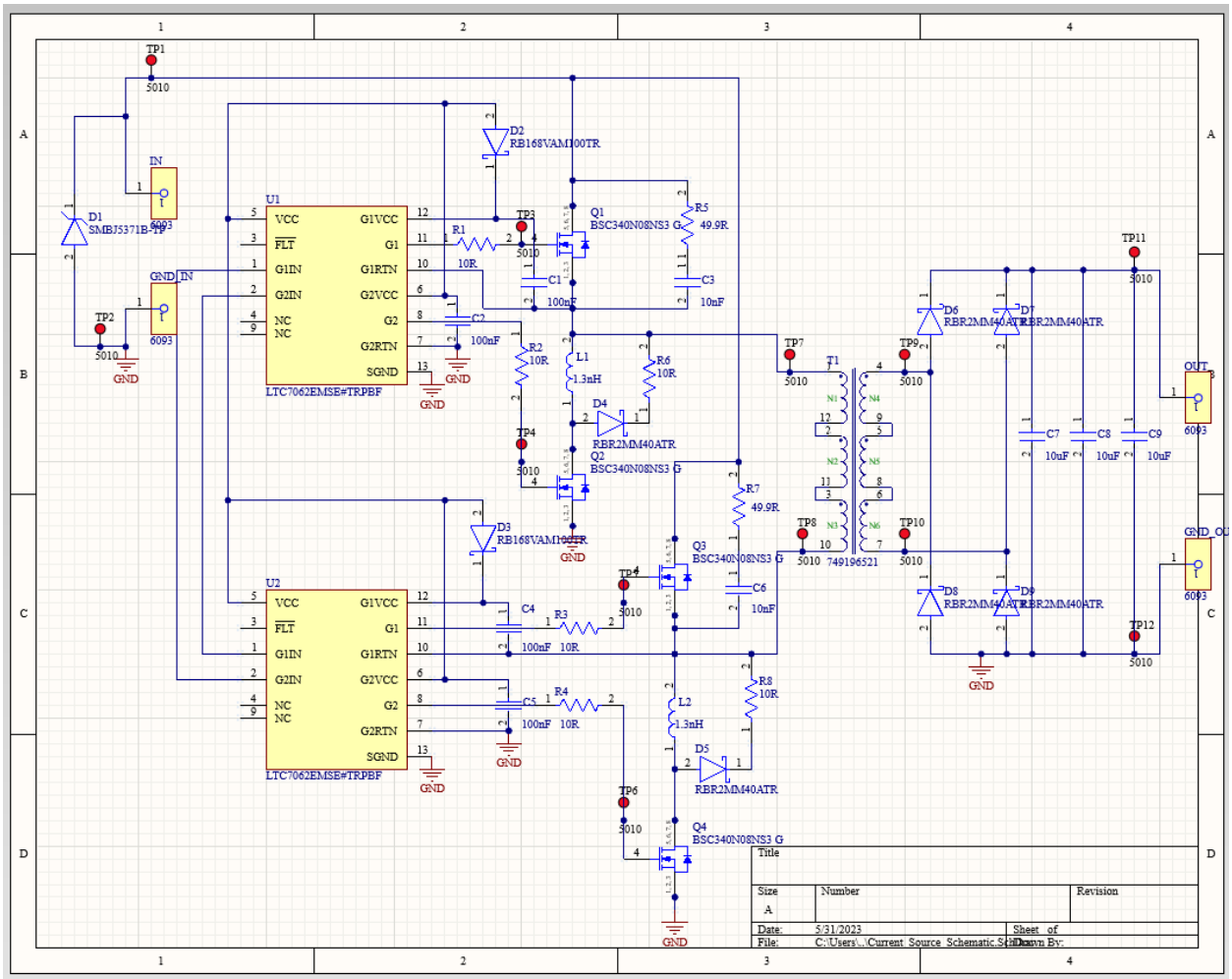

Figure 4-6: PCB Schematic

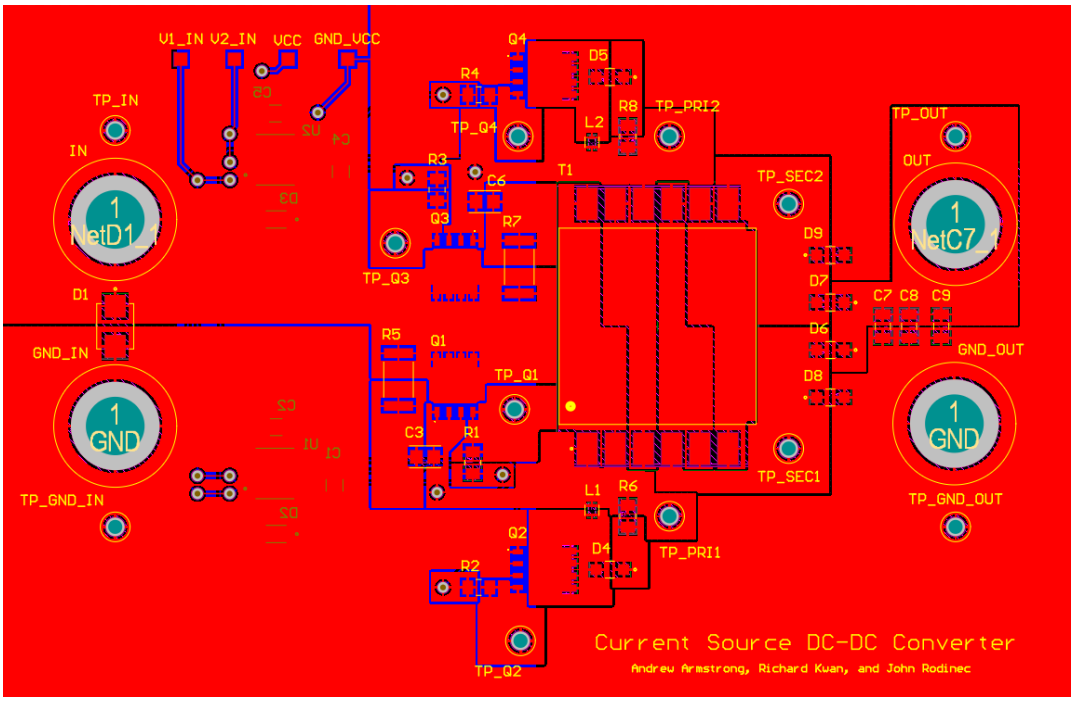

Figure 4-7: Top layer (red) of PCB layout

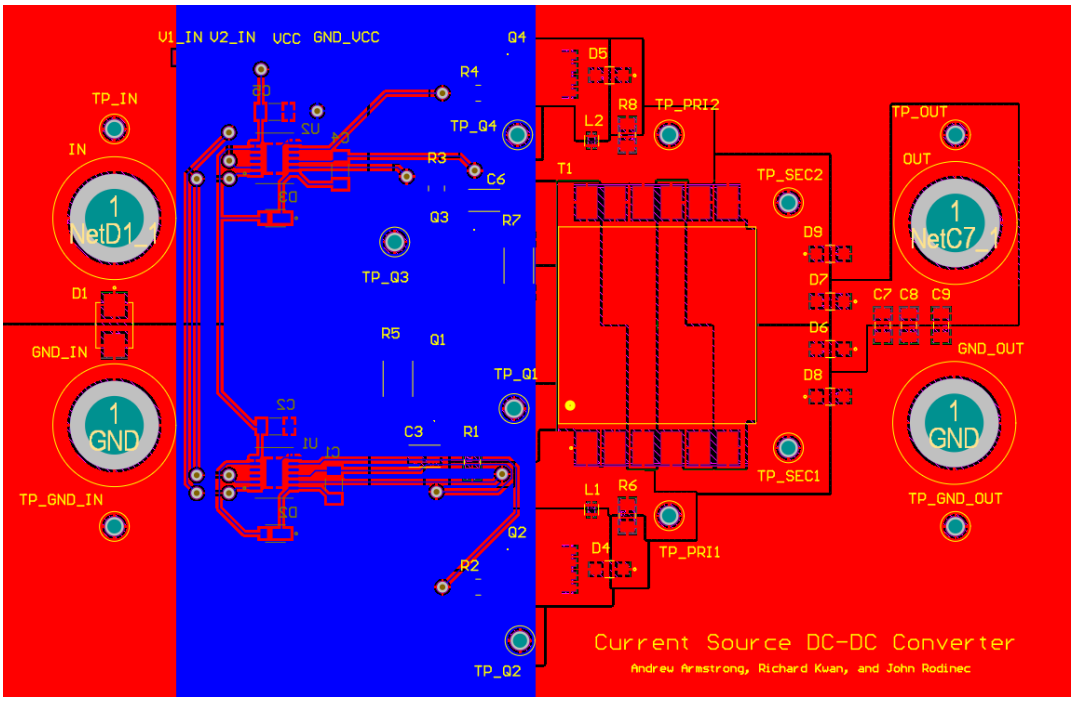

Figure 4-8 Bottom layer: (blue) of PCB layout

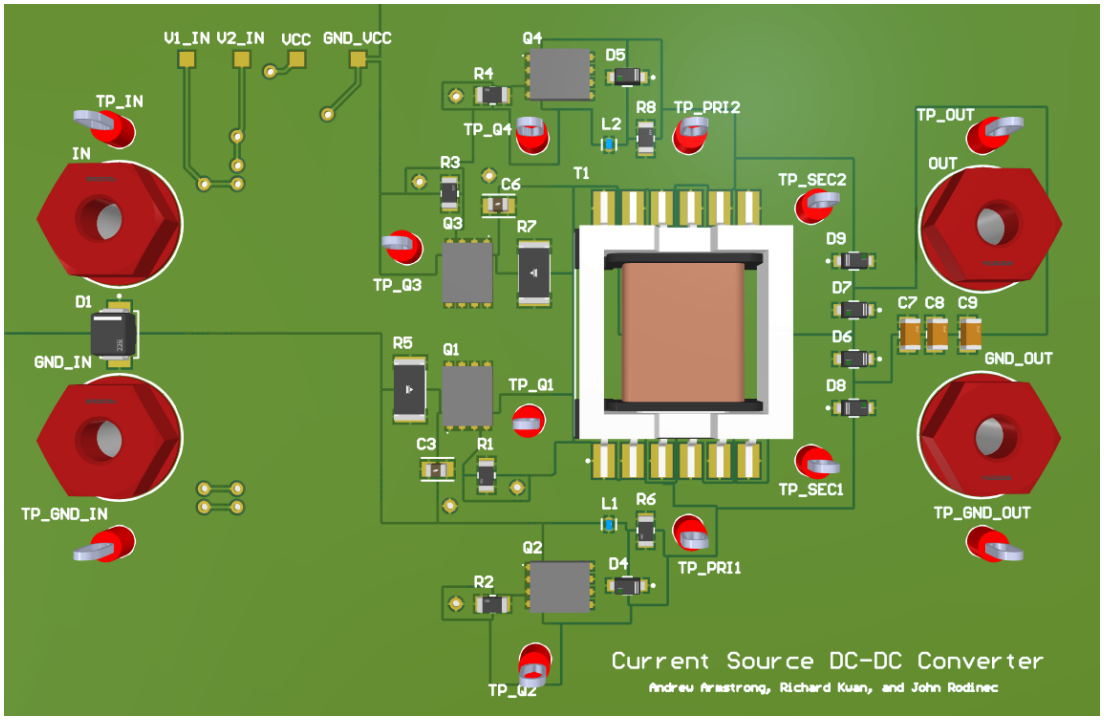

Figure 4-9: 3D top layer of PCB layout

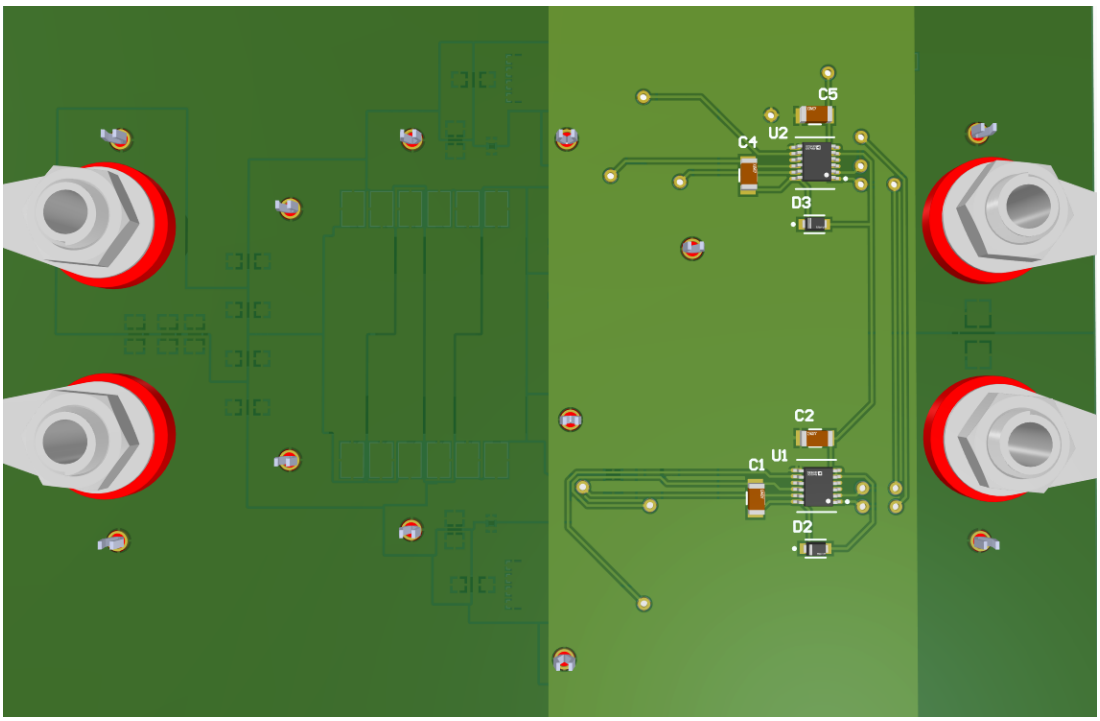

Figure 4-10: 3D bottom layer of PCB layout

Chapter 5. Hardware Test and Results

Construction of the hardware involved soldering the components onto the PCB. The finished product is shown in Figure 5-1. Once construction was completed, various tests were performed on the device in order to determine operational characteristics.

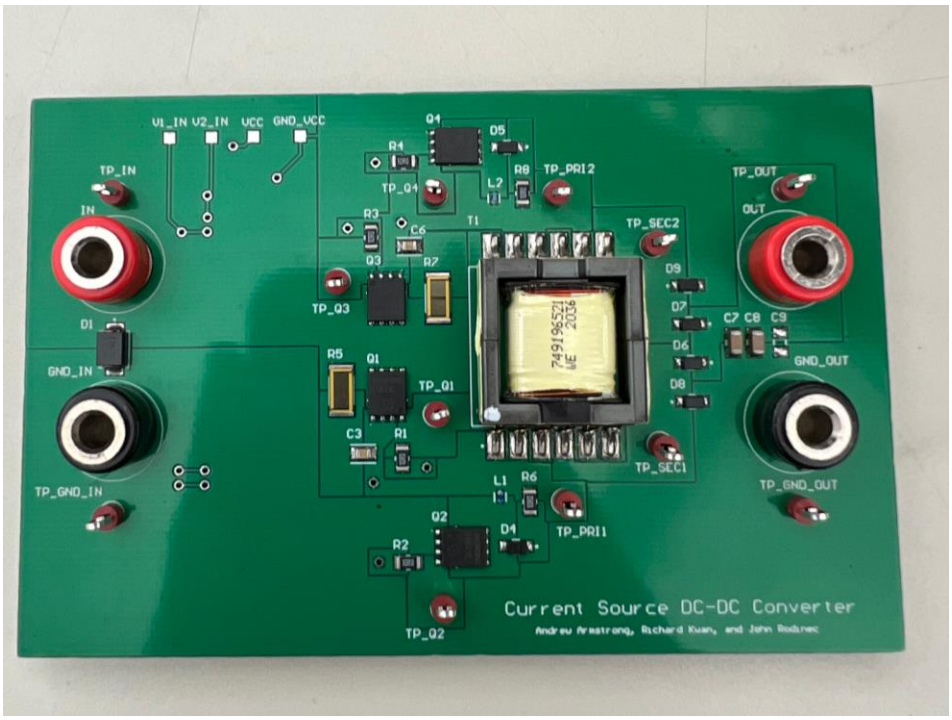

Figure 5-1: Finished PCB

The first set of tests were conducted with a setup represented in Figure 5-2. In absence of a current source power supply, a voltage source power supply was used in current limiting mode to control the current. This necessitated loading the power supply sufficiently to ensure that a stable current would be maintained. Generation of the gate signals was accomplished using a dual-channel function generator with both channels coupled to the same frequency. The channels were set to be 180 degrees out of phase using the generator's phase alignment function. A decade resistor box was used as a load. A digital multimeter and oscilloscope were attached to the converter's output to observe the output voltage.

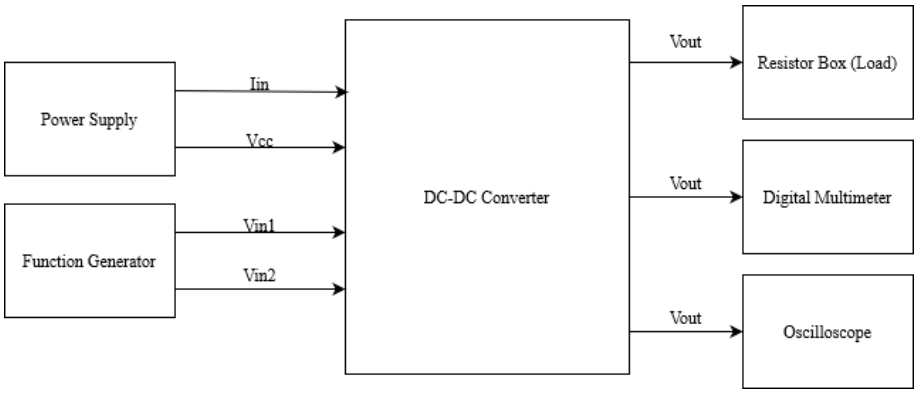

Figure 5-2: Block diagram of hardware test setup

The first measurement was observing the behavior of the converter in response to changes in the duty cycle of the switching signals. The load resistance was held constant at 38 ohms and the input current was held constant at 0.9 A. Using a two-channel function generator, the duty cycle of the switching signals were swept from 53% to 58%, and the output voltage across the output terminals was measured using a digital multimeter. The results of these measurements are tabulated in Table 5-1. It was observed that under nominal load conditions, the desired output voltage was achieved at a duty cycle of 53.5%.

Table 5-1: Output Voltage vs. Duty Cycle (R_L = 38 **Ω**, I_{IN} = 0.9 A)

Duty Cycle [%]	Output Voltage [V]
53	24.23
54	22.91
55	21.59
56	20.48
57	19.37
58	18.28
59	17.35
60	16.64

It was established that duty cycle and output voltage are inversely correlated. This is because a higher duty cycle results in more overlap between the gate signals. When the gate signals overlap, the primary winding of the transformer is shorted and no power is delivered to the transformer. It should be noted that the duty cycle cannot be lower than 50% to prevent the input current from being interrupted. Figure 5-3 visualizes this relationship.

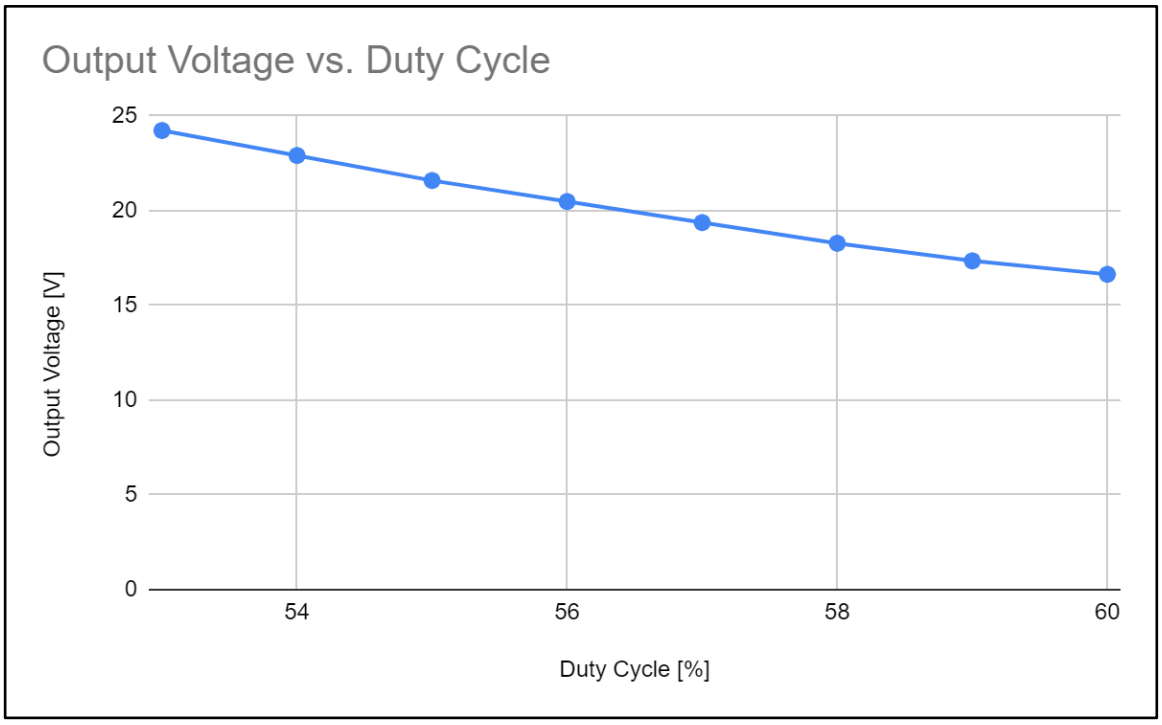

Figure 5-3: Effect of duty cycle on output voltage

The next measurement was observing the behavior of the converter as the input current was modified. Load resistance was held constant at the nominal value of 38 ohms and the duty cycle was held constant at 53.5%. Using the power supply, the input current was swept from 0.6 A to 0.9 A in steps of 0.05 A. The output voltage was measured across the output terminals of the converter. The results of these measurements are tabulated in Table 5-2.

Table 5-2: Output Voltage vs. Input Current (R_L = 38 Ω, 53.5% Duty Cycle)

Input Current [A]	Output Voltage [V]
0.6	15.86
0.65	17.19
0.7	18.53
0.75	19.82
0.8	21.11
0.85	22.38
0.9	24.12

It was established that there is a positive correlation between the value of the current and the output voltage when all other parameters are held constant. This is expected, as a larger input current means that the amount of power delivered to the transformer is higher, and thus more power is delivered to the load. This relationship is visualized in Figure 5-4.

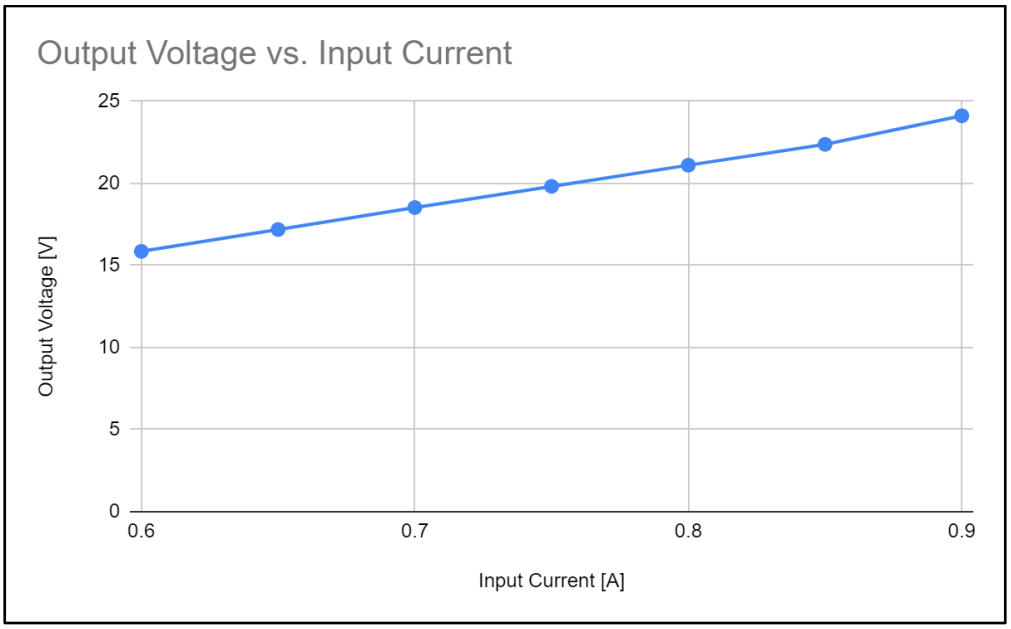

Figure 5-4: Effect of input current on output voltage

The last measurement in this testing configuration was observing the behavior of the converter as the load resistance was varied. Input current was held constant at the nominal value of 0.9 A and the duty cycle was held constant at 53.5%. Using the decade resistor box, different load values from 32 to 44 ohms were used in steps of 2 ohms. The output voltage was measured across the output terminals.

Table 5-3: Output Voltage vs. Load Resistance (I_{IN} = 0.9 A, 53.5% Duty Cycle)

Load Resistance [Ω]	Output Voltage [V]
32	20.58
34	21.63
36	22.71
38	23.60
40	25.30
42	26.09
44	26.91

It was established that the load resistance has a positive correlation with the output voltage when all other parameters are held constant. This is the expected behavior, as the current exiting the secondary winding of the transformer is the same as the input current regardless of load resistance. Thus, a higher load resistance will see a higher voltage across it. The relationship between output voltage and load resistance is visualized in Figure 5-5.

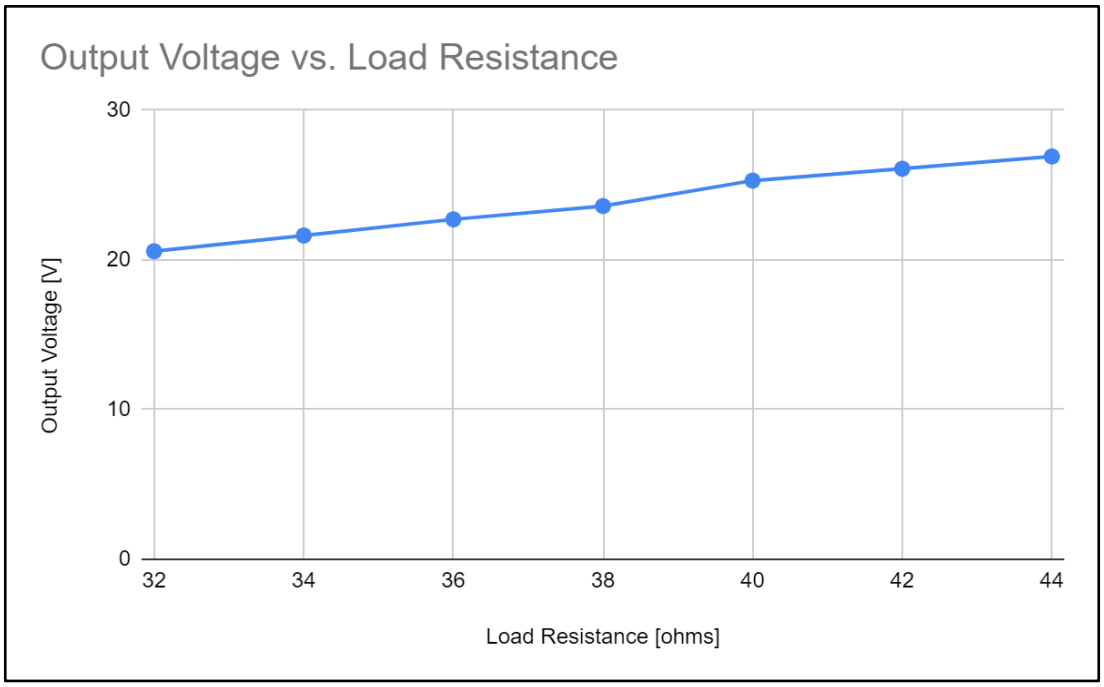

Figure 5-5: Effect of load resistance on output voltage

The efficiency testing of the converter was conducted by using the same setup as the previous tests except that the decade resistor box was replaced with an electronic load. The electronic load was configured to be in constant current mode. The equipment configuration for this test is shown in Figure 5-6.

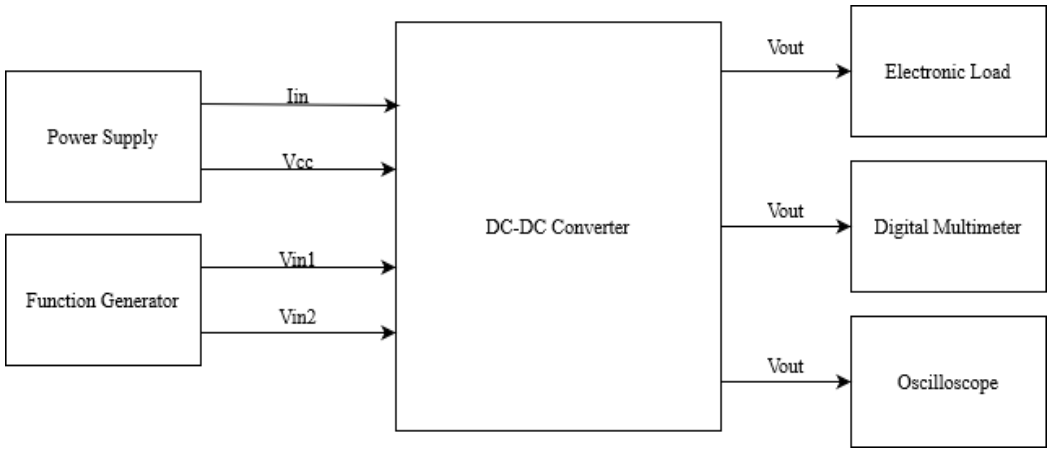

Figure 5-6: Block diagram of efficiency test

Due to the limitations imposed by not having a current-source power supply, the lower load currents were unable to load the power supply sufficiently such that the input current remained at 0.9 A. Furthermore, while ideally there would be a feedback controller to adjust the duty cycle such that the output voltage maintained 24 V, there was no such subsystem and the duty cycle was held at a fixed value. Attempts to measure the output voltage resulted in readings in excess of 30 V even with duty cycle adjustment. This may have been due to the electronic load being behaviorally different from the decade resistor box. Thus, the test continued with only adjustments to the load current. Efficiency was calculated by measuring the voltage and current at the converter terminals and calculating the ratio between output power and input power. The results are tabulated in Table 5-4.

Table 5-4: Converter Efficiency

Load Current [A]	Efficiency [%]
0.20	49.81
0.25	54.46
0.30	58.14
0.35	61.12
0.40	63.59
0.45	65.69
0.50	67.64
0.55	68.62
0.60	69.33
0.625	70.40

Although the procedure of obtaining this data was insufficient due to missing equipment and systems, it still shows that the converter is more efficient at larger loads. This is expected, as resistive snubbers are present on the input side of the converter. These snubbers always dissipate a fixed amount of power regardless of the load, so a smaller load would mean that the snubbers would represent a larger proportion of the power dissipated by the system. The efficiency curve is visualized in Figure 5-7.

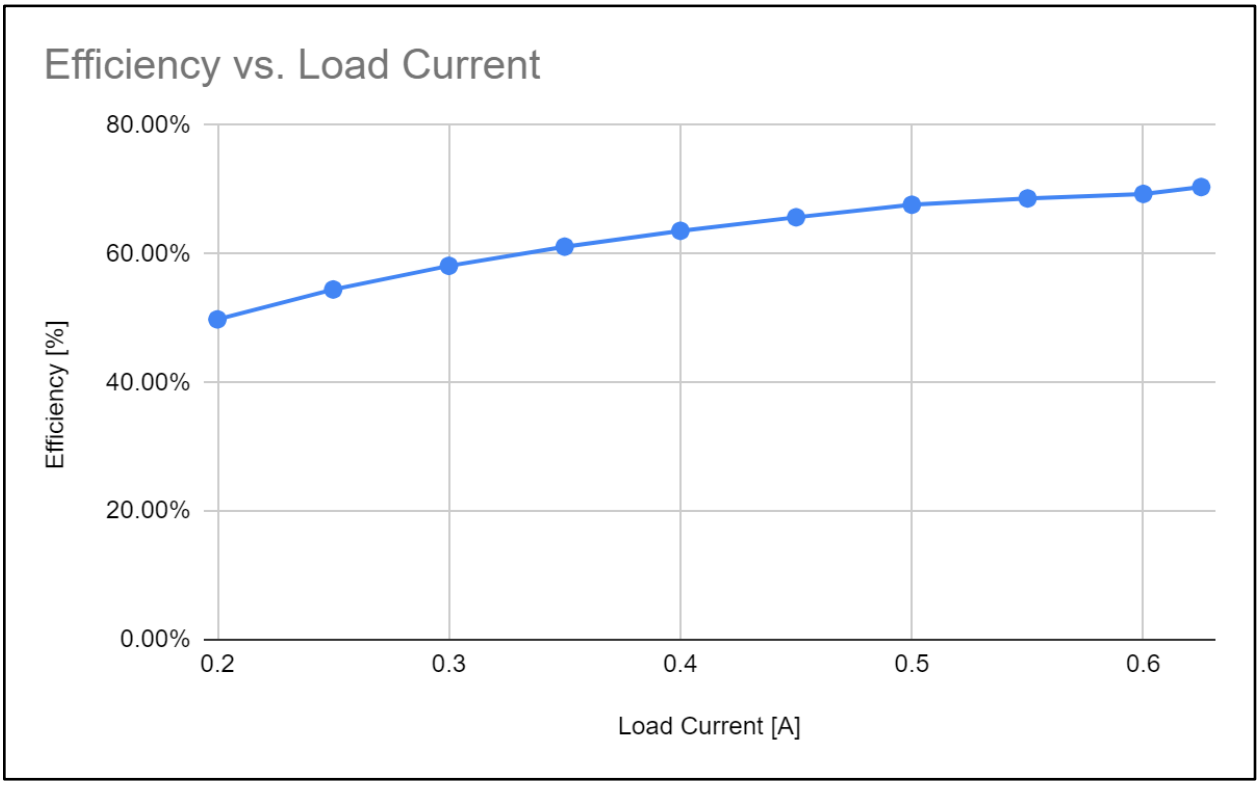

Figure 5-7: Efficiency curve of converter

The output terminals of the converter were connected to the oscilloscope to observe the quality of the output voltage waveform. The voltage ripple was observed to be around 4 volts peak-to-peak at a frequency of 500 kHz. This gives an output ripple percentage of 16.7%. As the frequency is twice that of the switching frequency, the voltage spikes are likely related to the rectifier. An image of the output voltage is shown in Figure 5-8.

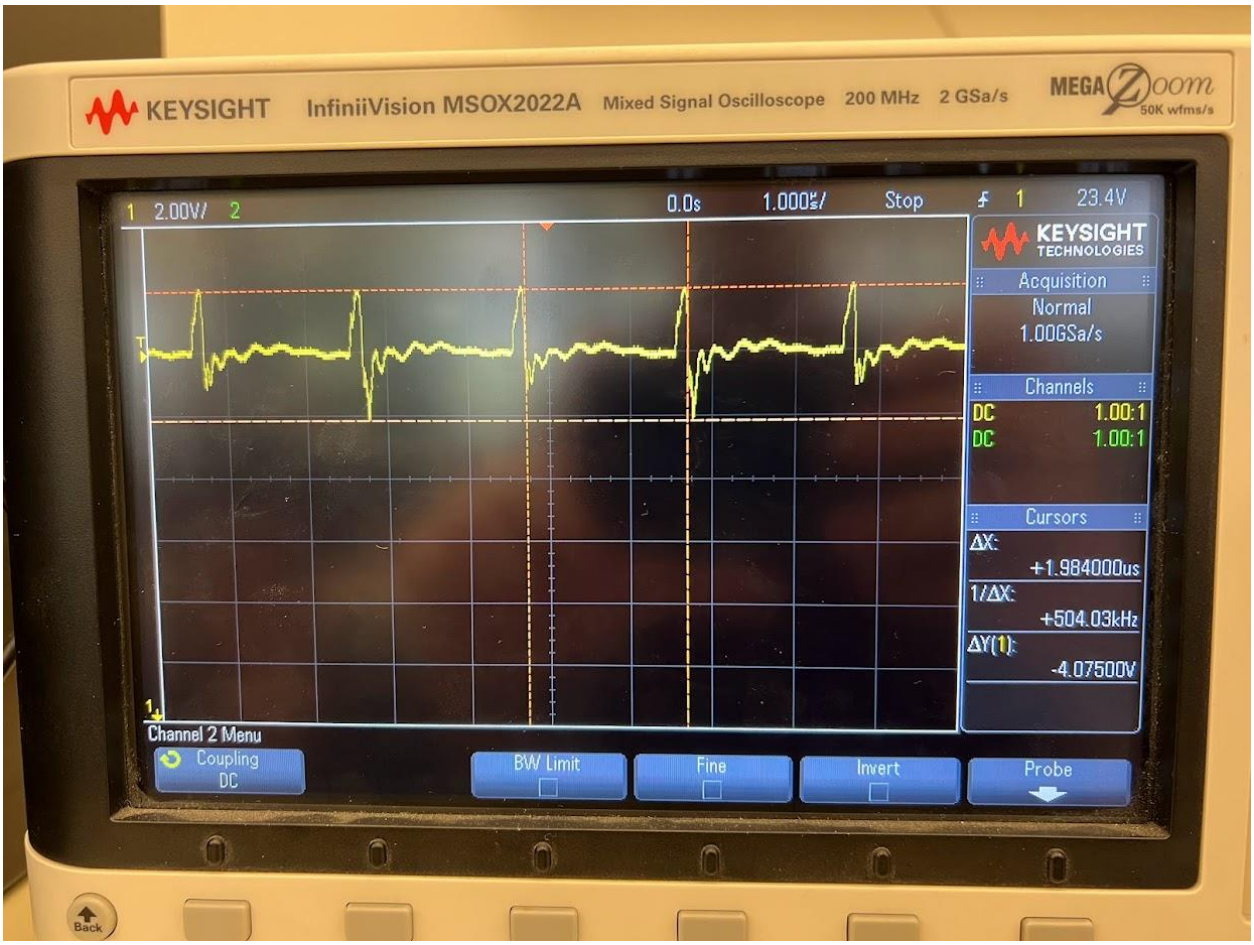

Figure 5-8: Output voltage ripple

While line and load regulations were design parameters that were considered in the conception of this project, they were not deemed suitable quantities to measure. Line regulation was not measured due to an inability to control the input voltage and given that the converter is current-sourced it did not make sense to measure this quantity. Load regulation was not measured because the lack of a feedback network meant that even with duty cycle adjustment, such a quantity would not be meaningful as manual changes to the duty cycle cannot realistically be implemented on a deployed device.

Chapter 6. Conclusion

The goal of this project was to create a current-source DC-DC converter that stepped down a 0.9A input current to a 0.625A output current at 24V. The designed circuit successfully stepped down the input current to the proper output, however the design did not meet the desired efficiency and output ripple specifications. Fortunately, the circuit provides a proof of concept of the current source design that can be iterated upon for better results in the future.

The first area of improvement for this design that would have a major impact on the performance of the device would be the inclusion of a feedback controller. The controller would monitor the output and adjust the duty cycle of the converter to maintain the proper output voltage. This would improve the overall quality of the DC output, as well as improve the efficiency of the device. As mentioned in Chapter 5, some tests, such as the efficiency test, are not completely accurate since the duty cycle could not accurately be varied to maintain a consistent output as the load changed. The addition of the controller would allow for more robust testing and the ability to diagnose future areas of improvement.

The overall performance of the circuit, such as the efficiency and output ripple, can also be improved through further tuning of the circuit. While efficiency would likely improve with the inclusion of a controller to regulate the output, certain components and designs could also be investigated to reduce losses. Designing a transformer could potentially result in less losses, as well as adjusting the component values of the snubber circuits. The voltage ripple may also be improved through the addition of more output capacitors.

Another area that could possibly see improvement is the test equipment. As mentioned in Chapter 5, the lack of a true current source led to difficulties with testing, which impacted the ability to accurately test the device and know about potential issues. Access to equipment that

could better model a current source could prove beneficial to proper testing of the device, but access to such equipment could be difficult and expensive.

Overall, this project successfully built upon previous projects in getting closer to a fully working prototype for a current-source DC-DC converter. This design successfully outputs the desired voltage and current, but a controller and further revisions are needed before the design can be fully realized.

References

[1]. J. Griffiths. “The global internet is powered by vast undersea cables. But they’re vulnerable.” CNN.com. https://www.cnn.com/2019/07/25/asia/internet-undersea-cables-intl-hnk (accessed Oct. 17, 2022)

[2]. T. Kaneko, Y. Chiba, K. Kunimi, T. Nakamura. “Very Compact and High Voltage Power Feeding Equipment (PFE) for Advanced Submarine Cable Network,” in *Suboptic 2010*, Yokohama, Japan, 2010. Available: https://web.archive.org/web/20200808071549/https://www.suboptic.org/wp-content/uploads/2014/10/255_Poster_EC_04.pdf.

[3]. *Submarine Cable Map* [Online]. Available: https://www.submarinecablemap.com/.

[4]. A. Varney. “Timeline History”. International Cable Protection Committee. https://www.iscpc.org/information/learn-about-submarine-cables/timeline-history/ (accessed Oct. 17, 2022).

[5]. R. Malaney, S. Gary. “Why is fibre optic technology 'faster' than copper?” ABC Science. https://www.abc.net.au/science/articles/2010/10/21/3044463.htm (accessed Oct.17, 2022).

[6]. TeleGeography. *Submarine Cable Frequently Asked Questions* [Online]. Available: https://www2.telegeography.com/submarine-cable-faqs-frequently-asked-questions

[7]. B. Lavallée. “To repeat, or not repeat, that is the question.” Ciena. https://www.ciena.com/insights/articles/to-repeat-or-not-repeat-that-is-the-question.html (accessed Oct. 17, 2022).

[8]. Y. Shohei, M. Satoshi, A. Ryuji, N. Toshihide. “The Optical Submarine Repeater and Its Associated Technologies,” *NEC Technical Journal*, vol. 5, pp. 13-17, 2010. Available: https://www.nec.com/en/global/techrep/journal/g10/n01/pdf/100104.pdf

[9]. S. Rahardjo. “Inovasi Teknologi Cable Based Tsunameter (InaCBT) untuk Kemandirian Teknologi dan Ketahanan Bencana Tsunami” Indonesia Tsunami Observation Center. http://www.inatoc.id/publikasi/documents/133/inovasi-teknologi-cable-based-tsunameter-inacbt-untuk-kemandirian-teknologi-dan-ketahanan-bencana-tsunami (accessed Oct. 17, 2022).

[10]. Xtera, “Xtera Repeater Datasheet,” Repeater Datasheet. Available: https://www.xtera.com/wp-content/uploads/2018/05/Xtera-Repeater-Datasheet-03-May-2018-1.pdf

[11]. Taufik, *Introduction to Power Electronics*, Lulu Publishing Inc., 2023.

[12]. F. Montalvo-Galicia, G. Diaz-Arango, C. Ventura-Arizmendi, B. Calvo and M. T. Sanz-Pascual, "Comparison of Two Internal Miller Compensation Techniques for LDO Regulators," 2019 16th International Conference on Electrical Engineering, Computing Science and Automatic Control (CCE), Mexico City, Mexico, 2019, pp. 1-4, doi: 10.1109/ICEEE.2019.8884571.

[13]. “Linear vs. Switching Regulators”, Renesas. [Online]. Available: https://www.renesas.com/us/en/products/power-power-management/linear-vs-switching-regulators.

[14]. “Definition of Switching Regulator”, Analog Devices. [Online]. Available: https://www.analog.com/en/design-center/glossary/switching_regulator.html.
[15]. A. Averberg and A. Mertens, "Analysis of a Voltage-fed Full Bridge DC-DC Converter in Fuel Cell Systems," 2007 IEEE Power Electronics Specialists Conference, Orlando, FL, USA, 2007, pp. 286-292, doi: 10.1109/PESC.2007.4342002.
[16]. A. K. Rathore, "Current-fed DC/DC converters for high voltage gain and low voltage high current applications: An overview of topologies and modulation techniques," 2016 IEEE International Conference on Power Electronics, Drives and Energy Systems (PEDES), Trivandrum, India, 2016, pp. 1-6, doi: 10.1109/PEDES.2016.7914439.
[17]. S. Ikeda and F. Kurokawa, "Isolated and wide input ranged boost full bridge DC-DC converter with low loss active snubber," 2017 IEEE Energy Conversion Congress and Exposition (ECCE), Cincinnati, OH, USA, 2017, pp. 2213-2218, doi: 10.1109/ECCE.2017.8096433.
[18]. J. C. Jose, “Current-Source DC-DC Converter for Fiber-Optic Communication Systems,” M.S. thesis, Dept. Elect. Eng., California Polytech. State Univ., San Luis Obispo, CA, USA, 2022. [Online]. Available: https://digitalcommons.calpoly.edu/theses/2453/
[19]. A. Adrian, C. Aguilar, and R. Sanchez, “Current-Source DC-DC Converter,” California Polytech. State Univ., San Luis Obispo, CA, USA, 2022. [Online]. Available: https://digitalcommons.calpoly.edu/eesp/561/
[20]. “Indonesia electricity prices.” Global Petrol Prices. https://www.globalpetrolprices.com/Indonesia/electricity_prices/. (accessed Nov. 27, 2022).

APPENDIX A — ANALYSIS OF SENIOR PROJECT DESIGN

Project Title: Current Source DC-DC Converter for Undersea Fiber Optic Sensors

Student's Name: Richard Kwan, Andrew Armstrong, John Rodinec

Advisor's Name: Taufik **Advisor's Initials:** **Date:**

Summary of Functional Requirements

This project is the design of a current source DC-DC converter to be used as a power supply for underwater fiber optic sensors. This design is intended to take an input current of 0.9 A and use high frequency switching to convert it to an output voltage of 24 V and an output current of 0.625 A.

Primary Constraints

A significant challenge in the design of this converter was obtaining accurate simulation models of a transformer to ensure that the behavior of the simulation was more accurate compared to using a simple coupled inductor model. This meant that the list of available transformers to pick from was severely limited, as many transformers do not come with SPICE models. Testing and evaluation was also difficult due to the lack of a feedback network to control the converter, and the lack of a proper current source to supply the input current. This resulted in suboptimal procedures and extreme difficulty in maintaining test conditions without causing potential damage to either the converter or the test equipment.

Economic

Human Capital

The converter would have a small effect in terms of human capital by creating some jobs related to the manufacture, marketing, and support of the devices. Because of their extremely

specific application it will likely be produced on an as needed basis and therefore the manufacturing side would not create many jobs. However, the marketing and support would be more active as marketing would always be reaching out to potential customers and support teams will provide assistance to existing customers.

Financial Capital

This product is targeted towards government organizations implementing a very specific type of cable-based tsunami detection system. The acquisition cost of the converter should not be excessively higher than the manufacturing cost because an unreasonable cost may result in a loss of interest in the project.

Natural Capital

The converter will be composed of, at minimum, passive components, integrated circuits, a transformer, and a PCB. The metals used will likely be reclaimable through specialized (and possibly expensive) recycling techniques, but the non-metallic materials will most likely not be recyclable. Realistically, even recycling the metals will not be economical unless the device is recycled as part of a batch of other unrelated, similar electronic devices.

The financial benefits of the project accrue in the use phase, as it is going to be used as a cheaper alternative to building entirely separate power feed systems. The cost will be split between acquisition and use, with the use phase having slightly more accrual of cost. This cost will be paid by the operator. Original estimates of manufacturing were placed at $50. The final manufacturing cost was $49.53. Operating profits on this project will be based on the cost difference between using this product instead of building and operating a separate power feed system, which currently has no cost estimate at this time. Given that the product still requires a few subsystems (such as a feedback controller) before becoming viable as a real-world system, it

will likely take one to two years before this product approaches a state suitable for deployment. Ideally, due to the difficulty in servicing these devices as a result of their use environment, these devices should last at least 5 to 10 years. See Appendix B for development timeframes.

If manufactured on a commercial basis:

As this converter will probably have low production volume due to its niche application, the purchase price will be higher at $80 to help recoup development costs.

Estimated number of devices sold per year: 30

Manufacturing cost for each device: $49.53

Estimated purchase price for each device: $80.00

Estimated profit per year: $914.10

The operating cost will vary depending on the electrical price of the user country. Assuming an efficiency of 70% and using Indonesia's average electricity price of 0.071 USD per kWh:

$$\$0.071 \text{ USD per kWh (Indonesia)} \times 21.4 \text{ W per unit} = \$0.00152 \text{ USD per unit per hour}$$

This is equivalent to a yearly operational cost of $13.32 USD per unit.

Environmental

Environmental impacts of use or manufacturing

The converter will be placed within a pressurized vessel at the sea floor. Should the converter be constructed using any toxic materials, they may end up leaching into the water if the pressure vessel fails and the converter is exposed to seawater. This can negatively affect the environment immediately around the converter. Thus, toxic materials should generally be avoided in the manufacturing of this device to minimize this risk.

Effects on natural resources and ecosystem services

As a product that contains electronics, this device will utilize various metals such as copper, aluminum, iron, etc. Depending on where the material is sourced, different types of mining techniques will be used. Some techniques are bound to be more environmentally harmful than others; steps should be taken to source electronics from reputable suppliers such that the materials are traceable.

Manufacturability

The demand for this product is low (due to it filling a very niche role), so the production volume

will be extremely limited. As a result, the devices will need to be assembled by hand as creating an assembly line with specialized tooling will not be cost effective.

Sustainability

In terms of in situ maintenance, the device will be difficult to maintain once deployed due to its application being at the bottom of the sea floor. Servicing the converter would involve physically raising the cable and opening the pressurized vessel that houses the converter. As mentioned prior, this project's use of resources will be based mainly on the sourcing of the components used; reputable suppliers should be used to ensure that materials are obtained sustainably. Upgrades to this design include improving the efficiency to minimize power loss in the use phase of the product. However, this may be difficult as a large portion of the power loss is likely in the switching snubbers, which are necessary in order to reduce unwanted voltage oscillations observed in simulations.

Ethical

The use of the device will be centered around IEEE Code of Ethics 1.1, as one of the converter's intended use cases will be part of a system that is intended to increase the safety of

people living near the coastlines of Indonesia. Misuse of the product would likely involve tampering with the converter such that it does not function, which would be immediately apparent when the sensor unit it is attached to is no longer connected to the network.

As mentioned in the prior impact categories, this device also has other ethical implications like sourcing components and materials from reputable distributors and minimizing the use of environmentally harmful materials in its construction. As before, this would revolve largely around IEEE Code of Ethics 1.1.

Health and Safety

One of the intended use cases for the sensors that will be powered by this converter is for tsunami detection. Failure of one or more converters will prevent the corresponding sensor units from collecting and transmitting data. This can result in a tsunami remaining undetected and posing a threat to coastal areas that have not been evacuated.

Social and Political

A potential inequality will be where these devices are implemented; because they must be co-located with fiber optic cables, communities that are not in proximity to these cable runs may not receive the benefit of such a system using these converters. In addition, the placement of the sensor units (and their power converters) as they are rolled out can become a point of political contention as local governments may vie for installation locations that are more relevant to them.

Development

A new technique learned by the students participating in this project was the generation of synchronized function generator outputs. In order to correctly supply the switching signals, the signals must be exactly 180 degrees out of phase. This was accomplished using function generators with phase alignment functionality.

Appendix B - Timeline of Tasks and Milestones

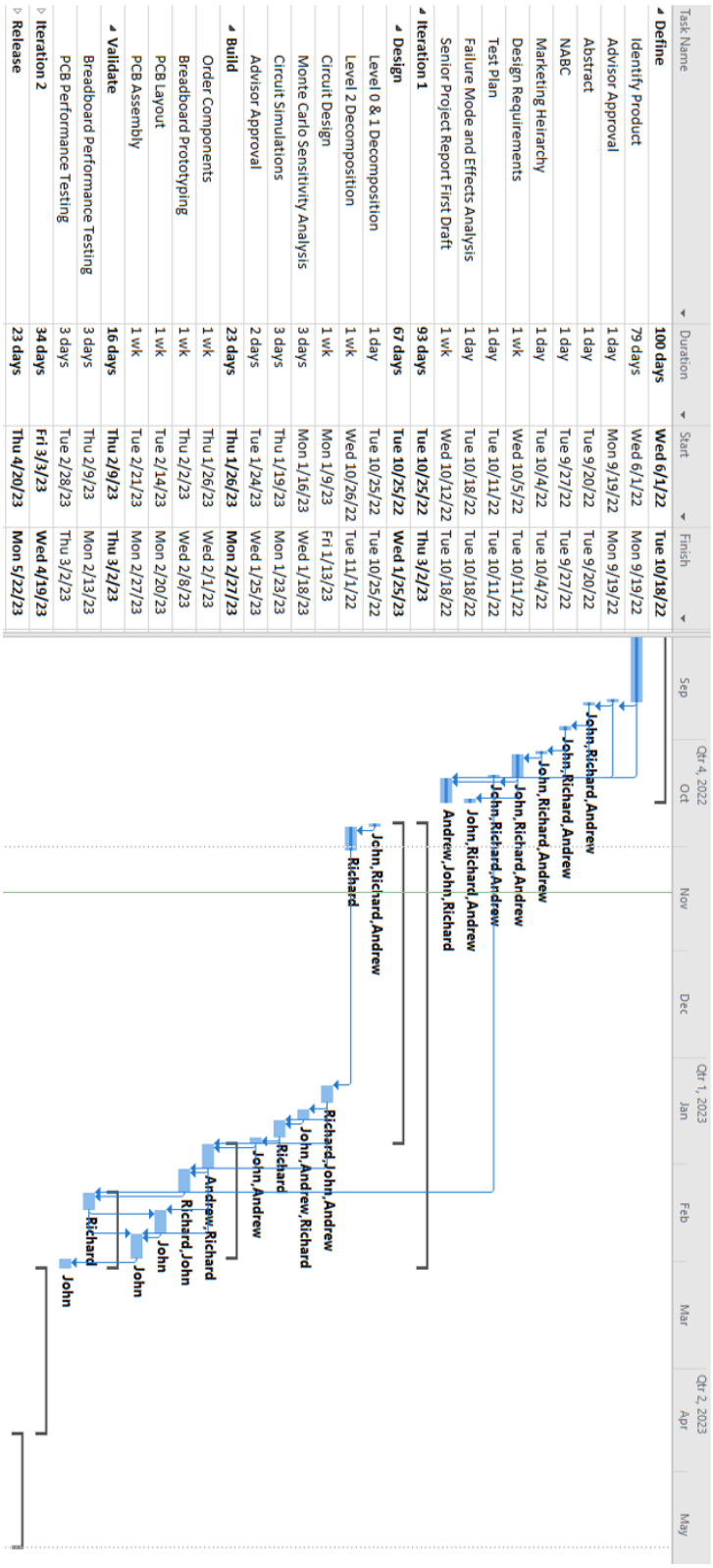

Task Name	Duration	Start	Finish
Define	**100 days**	**Wed 6/1/22**	**Tue 10/18/22**
Identify Product	79 days	Wed 6/1/22	Mon 9/19/22
Advisor Approval	1 day	Mon 9/19/22	Mon 9/19/22
Abstract	1 day	Tue 9/20/22	Tue 9/20/22
NABC	1 day	Tue 9/27/22	Tue 9/27/22
Marketing Heirarchy	1 day	Tue 10/4/22	Tue 10/4/22
Design Requirements	1 wk	Wed 10/5/22	Tue 10/11/22
Test Plan	1 day	Tue 10/11/22	Tue 10/11/22
Failure Mode and Effects Analysis	1 day	Tue 10/18/22	Tue 10/18/22
Senior Project Report First Draft	1 wk	Wed 10/12/22	Tue 10/18/22
Iteration 1	**93 days**	**Tue 10/25/22**	**Thu 3/2/23**
Design	**67 days**	**Tue 10/25/22**	**Wed 1/25/23**
Level 0 & 1 Decomposition	1 day	Tue 10/25/22	Tue 10/25/22
Level 2 Decomposition	1 wk	Wed 10/26/22	Tue 11/1/22
Circuit Design	1 wk	Mon 1/9/23	Fri 1/13/23
Monte Carlo Sensitivity Analysis	3 days	Mon 1/16/23	Wed 1/18/23
Circuit Simulations	3 days	Thu 1/19/23	Mon 1/23/23
Advisor Approval	2 days	Tue 1/24/23	Wed 1/25/23
Build	**23 days**	**Thu 1/26/23**	**Mon 2/27/23**
Order Components	1 wk	Thu 1/26/23	Wed 2/1/23
Breadboard Prototyping	1 wk	Thu 2/2/23	Wed 2/8/23
PCB Layout	1 wk	Tue 2/14/23	Mon 2/20/23
PCB Assembly	1 wk	Tue 2/21/23	Mon 2/27/23
Validate	**16 days**	**Thu 2/9/23**	**Thu 3/2/23**
Breadboard Performance Testing	3 days	Thu 2/9/23	Mon 2/13/23
PCB Performance Testing	3 days	Tue 2/28/23	Thu 3/2/23
Iteration 2	**34 days**	**Fri 3/3/23**	**Wed 4/19/23**
Release	**23 days**	**Thu 4/20/23**	**Mon 5/22/23**

Task Name	Duration	Start	Finish
Define	**100 days**	**Wed 6/1/22**	**Tue 10/18/22**
Iteration 1	**93 days**	**Tue 10/25/22**	**Thu 3/2/23**
Iteration 2	**34 days**	**Fri 3/3/23**	**Wed 4/19/23**
Design	**10 days**	**Fri 3/3/23**	**Thu 3/16/23**
Circuit Redesign	1 wk	Fri 3/3/23	Thu 3/9/23
Sensitivity Analysis	3 days	Fri 3/10/23	Tue 3/14/23
Simulations	3 days	Fri 3/10/23	Tue 3/14/23
Advisor Approval	2 days	Wed 3/15/23	Thu 3/16/23
Build	**18 days**	**Fri 3/17/23**	**Tue 4/11/23**
Breadboard Prototyping	1 wk	Fri 3/17/23	Thu 3/23/23
PCB Layout	1 wk	Wed 3/29/23	Tue 4/4/23
PCB Assembly	1 wk	Wed 4/5/23	Tue 4/11/23
Validate	**19 days**	**Fri 3/24/23**	**Wed 4/19/23**
Breadboard Performance Testing	3 days	Fri 3/24/23	Tue 3/28/23
PCB Testing	**6 days**	**Wed 4/12/23**	**Wed 4/19/23**
Peformance Tests	3 days	Wed 4/12/23	Fri 4/14/23
Vibration Tests	3 days	Mon 4/17/23	Wed 4/19/23
Environmental Tests	3 days	Mon 4/17/23	Wed 4/19/23
Release	**23 days**	**Thu 4/20/23**	**Mon 5/22/23**
Demonstration to Advisor	3 days	Thu 4/20/23	Mon 4/24/23
Prepare Senior Project Expo Board	2 wks	Tue 4/25/23	Mon 5/8/23
Final Report	2 wks	Tue 5/9/23	Mon 5/22/23

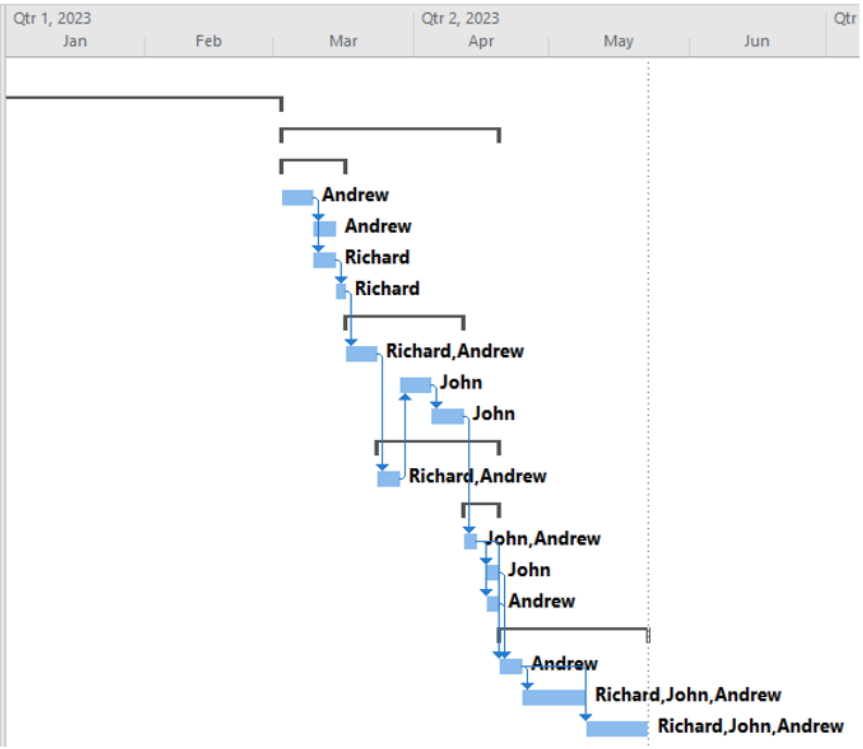

Appendix C - Bill of Materials

Table C-1: Bill of Materials

Part	Description	Size/Footprint	Unit Price	Quantity	Total Cost
LTC7062EMSE	Dual MOSFET Gate Driver	12-TSSOP	3.43	2	6.86
BSC340N08NS3GATMA1	N-Channel MOSFET, 80V	8-PowerTDFN	0.92	4	3.68
RB168VAM100TR	Schottky 100V 1A	2-SMD, FlatLead	0.42	2	0.84
RBR2MM40ATR	Schottky 40V 2A	SOD-123F	0.45	6	2.7
SMBJ5371B-TP	Zener 60V	DO214AA	0.48	1	0.48
749196521	Transformer, 12uH 1.7A 500VDC		10.32	1	10.32
RNCP1206FTD10R0	Resistor, 10 Ohm 1/2W +/-1%	1206	0.1	6	0.6
PCAN2512E49R9BST5	Resistor, 49.9 Ohm 6W +/0.1%	2512	7.69	2	15.38
12065C104KAT2A	Capacitor, 0.1uF 50V +/-10%	1206	0.17	4	0.68
CL21B103KCANNNC	Capacitor, 10nF 100V +/-10%	0805	0.1	2	0.2
CL31A106KBHNNNE	Capacitor, 10uF50V +/-10%	1206	0.33	3	0.99
LQW15AN1N3C80D	Inductor, 1.3nH +/-0.2nH 3.15A	0402	0.22	2	0.44
WMYCONGCONG	Banana Jack, External Thread		0.45	4	1.8
5010	Test Point, Red		0.38	12	4.56
					49.53